Title

RESONANCE RAMAN STUDIES IN Cu2O:I. THE PHONON-ASSISTED 1s YELLOW EXCITIONIC ABSORPTION EDGE

Author

Yu, Peter Y.

Publication Date

1975-04-01

Submitted to Physical Review

LBL-3901
Preprint c.1

RESONANCE RAMAN STUDIES IN Cu_2O:I. THE PHONON-ASSISTED 1s YELLOW EXCITONIC ABSORPTION EDGE

Peter Y. Yu and Y. R. Shen

April 1975

Prepared for the U. S. Energy Research and
Development Administration under Contract W-7405-ENG-48

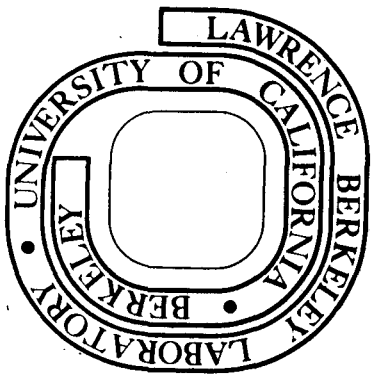

DISCLAIMER

Submitted to The Physical Review LBL-3901

UNIVERSITY OF CALIFORNIA

Lawrence Berkeley Laboratory
Berkeley, California

AECCContract No. W-7405-eng-48

RESONANCE RAMAN STUDIES IN Cu_2O:I. THE PHONON-ASSISTED 1s YELLOW EXCITONIC ABSORPTION EDGE*

Peter Y. Yu and Y. R. Shen

April 1975

* Supported in part by the U.S.E.R.D.A.

RESONANCE RAMAN STUDIES IN Cu_2O:I. THE PHONON-ASSISTED 1s YELLOW EXCITONIC ABSORPTION EDGE

by

Peter Y. Yu

Department of Physics, University of California

and

Inorganic Materials Research Division

Lawrence Berkeley Laboratory, Berkeley, California 94720

and

IBM Thomas J. Watson Research Center

Yorktown Heights, New York 10598†

and

Y. R. Shen

Department of Physics, University of California

and

Inorganic Materials Research Division

Lawrence Berkeley Laboratory, Berkeley, California 94720

ABSTRACT: Resonant Raman scattering in Cu_2O has been studied at low temperature in the vicinity of its phonon-assisted 1s yellow excitonic absorption edges using a cw, continuously tunable dye laser. The multi-phonon Raman modes which show resonance enhancement in this region are the following: $\Gamma_{12}^- + P$ (where P is an odd-parity optical phonon); $2\Gamma_{12}^- + P$ (where P is an acoustic or odd-parity optical phonon); $2\Gamma_{12}^- + 2LA$ and $4\Gamma_{12}^-$.

The Raman cross-sections of these modes have been calculated using perturbation theory. To explain the dispersion in the experimental cross-section it was found necessary to introduce a wave-vector dependent damping

constant for the 1s yellow exciton. A simple model proposed earlier by Yu, Shen, Petroff and Falicov was used to calculate this damping constant. Our result showed that the damping is predominantly due to intraband scattering via the longitudinal acoustic (LA) phonon. Good agreement was found between experiment and theory. Our result also indicate that the resonant three- and four-phonon Raman processes in Cu_2O in this region involve cascading of the photoexcited 1s yellow exciton with emission of phonon(s).

The Raman frequencies of some of the modes of Cu_2O were found to depend on the incident laser frequency. The behavior of these dispersive Raman modes were found to be well-explained within the above model and enabled us to determine directly the effective mass of the 1s exciton to be $(3.0 \pm 0.2)\ m_o$ (where m_o is the free mass of electron).

Relative magnitudes of various 1s exciton-phonon interactions have also been obtained from our result.

†Present address.

When the energy of photons used to excite Raman scattering in a medium is resonant with some electronic transitions of the medium, one expects in general the Raman cross-sections to be enhanced. This phenomenon is known as Resonance Raman Scattering (RRS)[1].

The study of RRS requires an intense, tunable and monochromatic source of light. As a result RRS experiments were first performed in solids with the Ar and Kr ion lasers[2]. These two lasers together with the He-Ne laser provide a total of approximately eighteen laser lines in the region of 6700 Å - 4500 Å with average separations of ∿ 100 Å. The discrete tuning of these lasers makes it difficult to study resonances whose widths are smaller than 100 Å and to make detailed lineshape analysis on the experimental result. These shortcomings have been overcome by the appearance of continuously tunable dye lasers[3]. We have made use of such a dye laser to study RRS in Cu_2O crystals. Our results will be presented in two papers of which the present paper is the first one. Some of the preliminary results have been reported in short communications[4-6].

Cu_2O is a particularly suitable candidate for RRS studies because within the tuning range of available dyes (5000 Å - 7000 Å) its optical spectra exhibit structures associated with quadrupole transitions, dipole transitions and phonon-assisted dipole transitions. This wealth of structures in the optical spectra is also reflected in its RRS results and provides a stringent test case of any theory on RRS. To explain our RRS results on Cu_2O we have found it necessary to modify existing RRS theories to take into account the dispersion in exciton damping constants[4] and effects due to multiple resonances[5]. We will also show how RRS can be very useful in providing new

information on phonons, excitons, and their interaction with each other.

In Section I we briefly review the relevant optical and lattice vibrational properties of Cu_2O and theories on RRS. In Section II we describe the experimental set-up and in Section III the RRS results of Cu_2O in the region of its phonon-assisted 1s yellow excitonic absorption edge. The results in the region of the yellow and green 2p, 3p,..., etc. excitonic series will be presented in the second paper. A detailed analysis and discussion of our results will be presented in Section IV.

SECTION I: REVIEW OF RELEVANT BACKGROUND MATERIALS

Band Structure, Lattice Vibration and Optical Properties of Cu_2O

Cuprous Oxide is one of the earliest crystals known to be a semiconductor. It crystallizes in a cubic lattice with two molecules per unit cell and space group O_h^4. Since it has inversion symmetry, its electronic and vibrational states all have definite parity. As we will see this inversion symmetry plays an important role in determining the properties of Cu_2O.

The optical properties of Cu_2O have been extensively studied by various authors.[7,8] At low temperatures its absorption spectrum exhibits a series of sharp lines associated with the creation of excitons. Depending on the photon energy region where they occur these exciton series are called the yellow, green, blue or indigo exciton series. Only the yellow and green series are accessible to our dye laser.

The yellow exciton series (see Figure 1) which arise from transition from the top valence band to the bottom conduction band at zone center satisfy the following equation:[8]

$$\nu_n = 17525 - 786\, n^{-2}\ \text{cm}^{-1} \quad n=2,3,... \qquad (1)$$

where ν_n is the frequency of the n^{th} exciton level.

The n=1 line of the series occurs at 16399.5 cm^{-1} and is very weak. This behavior of Cu_2O has been explained by Elliot[9] who suggested that the lowest conduction and top valence band of Cu_2O have the same parity. As a result only p states of the exciton formed from these bands can be excited by electric-dipole transitions.[10] The 1s line, which can only be excited by electric-quadrupole or magnetic-dipole transition, is therefore extremely weak. The validity of Elliot's theory has been confirmed by various experiments and by band structure calculation.

Electric-dipole excitation of the forbidden 1s yellow exciton is possible with the cooperation of a phonon with the right symmetry and parity. This phonon-assisted excitation of the 1s exciton gives rise to an absorption continuum beginning at $\sim$ 16500 cm^{-1} (at 4.2°K)[11]. Careful studies have revealed several steps in this absorption continuum corresponding to the participation of different phonons.

The lattice dynamics of Cu_2O have been studied by a number of authors[12]. It can be shown that Cu_2O possesses 15 zone-center optical phonons with symmetry:

$\Gamma_{15}^{-(1)}$, $\Gamma_{15}^{-(2)}$ which are infrared-active;

Γ_{25}^{+} which is Raman active and

Γ_{25}^{-}, Γ_{2}^{-} and Γ_{12}^{-} which are silent modes.

Group theoretical analysis predicts that phonons with symmetry: Γ_{25}^{-}, Γ_{15}^{-}, Γ_{2}^{-} and Γ_{12}^{-} can assist in the dipole excitation of the 1s exciton. Experimentally it was found that the phonon-assisted absorption edge of

Cu_2O was dominated by the contribution of the Γ_{12}^- phonon[9]. From the absorption measurements the energy of the zone-center Γ_{12}^- phonon was found to be $\sim$105 cm^{-1}. Table 1 gives the energies of the zone-center optical phonons of Cu_2O as determined by infrared absorption[13], photoluminescence[14] and resonant Raman scattering[15]. They are in good agreement with theoretical calculations by Carabatos and Prevot[12].

Theory of Resonance Raman Scattering

Using time-dependent perturbation theory one can obtain the first order Raman (Stokes) scattering probability per unit time as[16]:

$$P = (2\pi/\hbar^6) \sum_f \left| \sum_{\alpha,\beta} \frac{\langle f|H_I|\beta\rangle\langle\beta|H_I|\alpha\rangle\langle\alpha|H_I|i\rangle}{(\omega_\alpha-\omega_\ell)(\omega_\beta-\omega_\ell)} \right|^2 \delta(\omega_\ell-\omega_s-\omega_o) \qquad (2)$$

where

$|i\rangle$ is the initial state consisting of an incident photon (with frequency ω_ℓ and momentum $\hbar\vec{k}_\ell$) and the electronic system of the solid in the ground state;

$|f\rangle$ is the final state in which an incident photon has been annihilated to create a phonon (energy $\hbar\omega_o$ and momentum $\hbar\vec{q}$) and a scattered photon energy $\hbar\omega_s$ and momentum $\hbar\vec{k}_s = \hbar\vec{k}_\ell - \hbar\vec{q}$. The electronic system of the solid remains in the ground state;

$|\alpha\rangle$ and $|\beta\rangle$ are intermediate states in which the electronic system is in an excited state:

and H_I is the interaction Hamiltonian which is the sum of the electron-phonon interaction (H_{EL}) and the electron-photon interaction (H_{ER}).

δ is the Dirac delta function.

Among the three H_I matrix elements in Eq. (2) the H_{ER} term contributes to two matrix elements while H_{EL} contributes to the remaining one. Thus by permutating the order in which H_{EL} and H_{ER} occurs, one obtains the following six terms:

$$P \sim \Big| \sum_{\alpha,\beta} \Big\{ \frac{\langle f|H_{ER}(\omega_s)|\beta\rangle\langle\beta|H_{EL}|\alpha\rangle\langle\alpha|H_{ER}(\omega_\ell)|i\rangle}{(\omega_\beta + \omega_o - \omega_\ell)(\omega_\alpha - \omega_\ell)} + \frac{\langle f|H_{ER}(\omega_\ell)|\beta\rangle\langle\beta|H_{EL}|\alpha\rangle\langle\alpha|H_{ER}(\omega_s)i\rangle}{(\omega_\beta + \omega_o + \omega_s)(\omega_\alpha + \omega_s)} + \frac{\langle f|H_{ER}(\omega_s)|\beta\rangle\langle\beta|H_{ER}(\omega_\ell)|\alpha\rangle\langle\alpha|H_{EL}|i\rangle}{(\omega_\beta + \omega_o - \omega_\ell)(\omega_\alpha + \omega_o)} + \frac{\langle f|H_{ER}(\omega_\ell)|\beta\rangle\langle\beta|H_{ER}(\omega_s)|\alpha\rangle\langle\alpha|H_{EL}|i\rangle}{(\omega_\beta + \omega_o + \omega_s)(\omega_\alpha + \omega_o)} + \frac{\langle f|H_{EL}|\beta\rangle\langle\beta|H_{ER}(\omega_s)|\alpha\rangle\langle\alpha|H_{ER}(\omega_\ell)|i\rangle}{(\omega_\beta + \omega_s - \omega_\ell)(\omega_\alpha - \omega_\ell)} + \frac{\langle f|H_{EL}|\beta\rangle\langle\beta|H_{ER}(\omega_\ell)|\alpha\rangle\langle\alpha|H_{ER}(\omega_s)|i\rangle}{(\omega_\beta + \omega_s - \omega_\ell)(\omega_\alpha + \omega_s)} \Big\} \Big|^2 \qquad (3)$$

Of these six terms the first one usually makes the strongest contribution towards RRS; so in most RRS theories the remaining terms are taken to be equal to a constant. If this constant background can be neglected, then we can write the Raman (Stokes) cross-section as:

$$R(\omega_\ell) \sim \sum_f \Big| \sum_{\alpha,\beta} \frac{\langle f|H_{ER}(\omega_s)|\beta\rangle\langle\beta|H_{EL}|\alpha\rangle\langle\alpha|H_{ER}(\omega_\ell)|i\rangle}{(\omega_\beta + \omega_o - \omega_\ell)(\omega_\alpha - \omega_\ell)} \Big|^2 \delta(\omega_\ell - \omega_s - \omega_o) \qquad (4)$$

The excited states α and β can consist of electron-hole pairs which may be free or correlated (excitons).

It is obvious from Eq. (4) that the Raman cross-section is enhanced when one of the energy denominators is small. For example if the solid has a sharp exciton ω_{ex} as an intermediate state, Eq. (4) predicts poles in $R(\omega_\ell)$ at $\omega_\ell = \omega_{ex}$ and at $\omega_s = \omega_{ex}$. When only one energy denominator in Eq. (4) vanishes, this resonance effect will be referred to as a single resonance. But one would expect a stronger resonance to occur when more than one energy denominator vanish simultaneously (multiple resonance). Whenever the electronic energy spectrum allows such multiple resonances we expect them to dominate the RRS.

In Eq. (4) $R(\omega_\ell)$ diverges when $\omega_\ell = \omega_\alpha$. This unphysical result can be avoided by a well-established procedure of introducing a damping constant to each denominator in Eq. (4).[17] We simply replace ω_α and ω_β in Eq. (4) by $\omega_\alpha + i\Gamma_\alpha$ and $\omega_\beta + i\Gamma_\beta$ where Γ_α and Γ_β are phenomenological damping parameters. Usually for simplicity reason the dampings of the intermediate states are assumed to be energy independent. However under the special circumstances one encounters in Cu_2O, it is necessary to consider the dispersion of the damping. It should be pointed out that if the interaction H_{ER} between the photon and exciton is strong enough it is necessary to treat the photon and exciton together as a coupled excitation (polariton)[18]. This is found to be not necessary in case of Cu_2O.

Because of parity selection rules, only the Γ_{25}^+ optical phonon can participate in one-phonon non-resonant Raman scattering[16]. The other modes

can, however, participate in overtone and combination scattering.[19]

In general there are three types of processes (shown diagrammatically in Figure 2) which contribute to two-phonon Raman scattering:[20]

(a) The incident photon excites the system to the intermediate state α which is scattered to another state β by emitting two phonons simultaneously. The system returns from β to the ground state with emission of the scattered photon.

(b) The incident photon excites the system to α which is scattered successively through the states β and γ. At each scattering one phonon is emitted. The system returns to the ground state from γ with emission of the scattered photon.

(c) The entire one phonon Raman scattering process is repeated twice.

The contributions of these three types of processes differ in magnitude and dispersion. In Cu_2O we will show that a combination of parity and resonance considerations makes type (b) the dominant process in two-phonon RRS. In a straightforward way one can generalize Eq. (4) to obtain the resonant Raman cross-section for a type (b) two-phonon scattering as:

$$R(\omega_\ell) \sim \left| \sum_{\alpha,\beta,\gamma} \frac{\langle f|H_{ER}(\omega_s)|\gamma\rangle\langle\gamma|H_{EL}(2)|\beta\rangle\langle\beta|H_{EL}(1)|\alpha\rangle\langle\alpha|H_{ER}(\omega_\ell)|i\rangle}{(\omega_\gamma + \omega_o(1) + \omega_o(2) - \omega_\ell)(\omega_\beta + \omega_o(1) - \omega_\ell)(\omega_\alpha - \omega_\ell)} \right|^2 \quad (5)$$

Here 1 and 2 refers to the two phonons involved.

SECTION II: EXPERIMENTAL SET-UP

Figure 3 shows a schematic diagram of the apparatus used in our experiment. The dye laser (Spectra Physics Model 70 or Coherent Radiation

Model 490) is pumped by an Ar ion laser. By using the dyes: Rhodamine 6G (dissolved in methanol and water of hexafluoroisopropanol) and Coumarin 6 (dissolved in Benzyl Alcohol) we obtained typical laser output > 30 mW and tunable continuously between 5250 Å and 6400 Å with halfwidth $\lesssim$ 0.5 Å. The dye laser beam contains a fluorescence back-ground $\sim$200 Å broad and centered on the dye laser wavelength. By using a combination of Brewster angle prisms and apertures we narrowed the total width of the fluorescence background to $\sim$30 Å with a loss of $\sim$30% in power.

The sample, after mechanical polishing and etching with dilute HNO_3, was placed either on the cold finger of a helium dewar or immersed in superfluid helium. In the former case the temperature of the sample was monitored by a calibrated carbon resistor thermometer placed immediately behind the sample inside the cold finger. To minimize heating up of the sample by the laser beam, a cylindrical lens was used to focus the laser on the sample. The back-scattered light was analyzed by a double monochromator and photon counting system. The intensity of the scattered radiation was normalized against the intensity of a Raman line of calcite measured under similar conditions.

Measurements have been performed on crystals prepared by two different methods: (a) by oxidation of high purity copper and (b) by pulling from a melt in an arc image furnace.[21] Samples prepared by method (a) have lower luminescence intensity while samples prepared by method (b) have higher luminescence intensity.[22] However, no difference was found between the Raman spectra of the two kinds of samples; so unless otherwise stated results reported in this paper have been obtained from samples prepared by method (a) (because the luminescence tends to mask the weak Raman lines).

Since our Cu_2O samples are not oriented along any high symmetry axes, no attempt has been made to study the selection rules of the Raman spectra. All Raman spectra discussed in this paper are unpolarized. Since we are studying multiphonon scattering in this paper we do not expect this limitation to affect our result and their interpretation in any serious way.

SECTION III. EXPERIMENTAL RESULTS

As pointed out in Section I the optical absorption in Cu_2O at its 1s yellow exciton, its phonon-assisted absorption edge and its yellow and green excitonic series all involve different processes. As a result the resonant Raman processes in these three regions are quite different too. At the 1s exciton the odd parity one-phonon Raman modes are strongly enhanced. The RRS in this region has been studied in detail by Compaan and Cummins.[15] In this paper we will be interested mainly in the phonon-assisted absorption edge. The yellow and green excitonic series will be covered in the second paper.

Figure 4 shows the Raman spectra of Cu_2O for three different incident photon energies. In Figure 4(a) the photon frequency is just below the absorption edge and in 4(b) and 4(c) above the absorption edge. It is obvious that there are more structures in Figures 4(b) and (c) than in 4(a). The broad structures in Figure 4(b) are due to luminescence. They can be distinguished from the Raman peaks by the fact that their frequencies are independent of the dye laser frequency. The result of our study on the luminescence spectra of Cu_2O will be published elsewhere.[22]

In Figure 5 we show the dispersion of the Raman cross-section of the strong 220 cm^{-1} mode. This is the only mode which can be observed over

the entire tuning range of our dye laser and at higher temperatures. In Figures 6 and 7 we show the dispersion of the other Raman peaks which have been identified as two-phonon, three-phonon and four-phonon modes. The identification of these modes will be discussed in the next section. In all the above figures the effect of absorption has been corrected for in the manner suggested by Loudon.[23]

It is well-known that Raman frequency shifts depend only on the medium and should be independent of the incident photon energy. However, we found that the frequency of a few of the Raman peaks of Cu_2O above the absorption edge varies with the dye laser frequency ω_ℓ. This is shown in Figure 8 where we have plotted the Raman frequencies and half-widths of all the observed peaks of Cu_2O between 180 cm^{-1} and 500 cm^{-1} as a function of ω_ℓ. We note that the peaks labelled Y and Z show dependence on ω_ℓ in both their frequencies and linewidths while the $\Gamma_{12}^- + \Gamma_{15}^{-(1)}$ modes exhibit a shift in frequency with ω_ℓ. A detailed analysis of these results will be presented in the next section.

SECTION IV: DISCUSSION

First we will address ourselves to the problem of identification of the various Raman lines observed in Cu_2O. According to group theory there should be only one Raman active phonon (Γ_{25}^+) whereas most authors observed a large number of lines.[13] This has led some authors to analyze the Raman spectra of Cu_2O in terms of local modes due to non-stoichiometry or impurities.

In this paper we will adopt the following approach in identifying the Raman lines of Cu_2O. First we have summarized in Table I the frequency of

the zone-center phonons of Cu_2O obtained by various methods. Resonant Raman scattering at the 1s exciton[15] and photoluminescence[14,22] provides the energy of all the odd-parity zone-center phonons. Infrared absorption gives the energies of the Γ_{15}^- modes.[13] The symmetries of these phonons, except for the Γ_{12}^- and infrared active Γ_{15}^- modes, are then assigned by comparison with the theoretical zone-center phonon energies calculated by Carabatos and Prevot.[12] From Table 1 one can see that the fairly good agreement between theory and experiment supports these assignments.

After establishing the zone-center phonon energies we found that most of the Raman lines of Cu_2O can be identified as multiphonon modes based entirely on their frequency. For example in Figure 4(b) we can assign the observed Raman modes as: (the corresponding frequencies calculated from Table 1 are shown in parenthesis)

$$198\ cm^{-1} : \Gamma_{25}^- + \Gamma_{12}^- \quad (195\ cm^{-1})$$

$$220\ cm^{-1} : 2\Gamma_{12}^- \quad (218\ cm^{-1})$$

$$265\ cm^{-1} : \Gamma_{12}^- + \Gamma_{15}^{-(1)}\ (LO) \quad (262\ cm^{-1})$$

$$460\ cm^{-1} : \Gamma_{12}^- + \Gamma_{2}^- \quad (459\ cm^{-1})$$

$$628\ cm^{-1} : \Gamma_{12}^- + \Gamma_{25}^+ \quad (624\ cm^{-1})$$

In many cases the RRS of a particular mode provides an additional check on the validity of the identification, especially when a line can be decomposed into a sum of phonons in several ways. Such a case would be the 307 cm^{-1} line in Figure 4(c). This line can be a $2\Gamma_{12}^- + \Gamma_{25}^-$ (304 cm^{-1}) or $2\Gamma_{15}^{-(1)}$ (LO) (306 cm^{-1}) mode. The RRS of this line suggests that for incident photon energy just above the absorption edge (as in Figure 4(c)) this line

is a $2\Gamma_{12}^- + \Gamma_{25}^-$ mode[6] while for photon energy close to the yellow excitonic series it is a $2\Gamma_{15}^{-(1)}$ (LO) mode.[5]

(1) RRS of Two-phonon Modes of Cu_2O: $\Gamma_{12}^- + P$ (where P is an odd parity Optical Phonon)

Since the $2\Gamma_{12}^-$ mode showed the strongest enhancement we will consider it first. As pointed out in Section I there are three types of Raman processes which can contribute to a two-phonon scattering. The following considerations shows that the RRS of the $2\Gamma_{12}^-$ mode is dominated by process (b) in Figure 2. Process (c) can be ruled out right away because one-phonon scattering of the Γ_{12}^- mode is forbidden. Experimentally we observe that the Raman cross-section of the $2\Gamma_{12}^-$ mode rises very abruptly at the absorption edge (see Figure 5). Since this absorption edge is due to photo-excitation of the 1s yellow exciton with emission of Γ_{12}^- phonons, this suggests that the two Γ_{12}^- phonons in the Raman process are emitted in two separate steps as in process (b). We note that in process (a) the two phonons are emitted simultaneously.

The Raman cross-section of a type (b) two-phonon process is given by Eq. (5). Consider the scattering of two Γ_{12}^- phonons with opposite wave vectors: $\vec{q}$ and $-\vec{q}$ (with energies $\hbar\omega_{12}(\vec{q})$ and $\hbar\omega_{12}(-\vec{q})$ respectively). We can assume the incident photon energy $\hbar\omega_\ell$ is close to the absorption edge in Figure 1 (the energy of this Γ_{12}^- phonon-assisted absorption edge is given by $\hbar\omega_1 + \hbar\omega_{12}$ (q=0) where $\hbar\omega_1$ is the energy of the 1s yellow exciton). The initial state $|i\rangle$ with no exciton or phonon is denoted by $|0;0;n_\ell,n_s\rangle$. The first two symbols in the 'ket' refer respectively to the exciton and phonon excited while the last two are the numbers of incident

(η_ℓ) and scattered photons (η_s). In the intermediate state $|\alpha\rangle$ an incident photon ω_ℓ has been destroyed in exciting an exciton $\underline{b}$ by electric dipole transition, so $|\alpha\rangle=|\underline{b};0;\eta_\ell-1;\eta_s\rangle$. The summation over α in Eq. (5) is now translated into a summation over all possible exciton states $\underline{b}$. However the frequency denominator $\omega_\alpha-\omega_\ell$ in Eq. (5), suggests that the largest contributions probably come from the low energy dipole-allowed excitons (namely, the blue and indigo excitons[8]). To reach the next intermediate state $|\beta\rangle$ the exciton $\underline{b}$ is scattered to another exciton $\underline{a}$ with emission of a Γ_{12}^- phonon ($\omega_{12}(\vec{q})$ or $\omega_{12}(-\vec{q})$ and for the time being we will assume $\omega_{12}(\vec{q})$ is emitted first). To conserve momentum exciton $\underline{a}$ must have momentum $-\hbar\vec{q}$. Again we have to sum over all possible excitons $\underline{a}$ but in this case contribution from the 1s yellow exciton $\omega_1(-\vec{q})$ dominates because the frequency denominator $\omega_\beta+\omega_{12}(\vec{q})-\omega_\ell = \omega_1(-\vec{q})+\omega_{12}(\vec{q})-\omega_\ell$ is small (since $\omega_\ell \sim \omega_1(0) + \omega_{12}(0)$). The 1s yellow exciton forms a resonant intermediate state in this case. Thus we can write $|\beta\rangle=|1s;\Gamma_{12}^-;\eta_\ell-1;\eta_s\rangle$. In the same notations we can write $|\gamma\rangle=|\underline{b}';2\Gamma_{12}^-;\eta_\ell-1;\eta_s\rangle$ and $|f\rangle=|0;2\Gamma_{12}^-;\eta_\ell-1;\eta_s+1\rangle$. $\underline{b}'$ stands for another dipole-allowed exciton which has to be summed over.

The total cross-section of the $2\Gamma_{12}^-$ mode is now obtained by summing Eq. (5) over the phonon density-of-states. This is given by (except for some constants of proportionality):

$$R_{2\Gamma_{12}^-}(\omega_\ell) \sim \sum_{\vec{q}} \Bigg| \sum_{\underline{b},\underline{b}'} \frac{\langle 0;2\Gamma_{12}^-;\eta_\ell-1;\eta_s+1|H_{ER}(\omega_s)|\underline{b}';2\Gamma_{12}^-;\eta_\ell-1;\eta_s\rangle}{\omega_{\underline{b}'}+\omega_{12}(\vec{q})+\omega_{12}(-\vec{q})-\omega_\ell} \times$$

$$\times \frac{\langle \underline{b}';2\Gamma_{12}^-;\eta_\ell-1;\eta_s|H_{ER}|1s;\Gamma_{12}^-;\eta_\ell-1;\eta_s\rangle}{\omega_1^0+(\hbar q^2/2M)+\omega_{12}(\vec{q})-\omega_\ell} \times$$

$$\times \frac{\langle 1s;\Gamma_{12}^-;\eta_\ell-1;\eta_s|H_{ER}|\underline{b};0;\eta_\ell-1;\eta_s\rangle\langle \underline{b};0;\eta_\ell-1;\eta_s|H_{ER}(\omega_\ell)|i;0;\eta_\ell;\eta_s\rangle}{\omega_{\underline{b}}-\omega_\ell}\Bigg|^2 \qquad (6)$$

where we have assumed that the 1s exciton band is spherical with $\omega_1(\vec{q}) = \omega_1^0 + \hbar q^2/2M$, M being the effective mass of the 1s yellow exciton. Equation (6) can be simplified under these assumptions:

(i) the Γ_{12}^- phonon has no dispersion, i.e. $\omega_{12}(\vec{q}) = \omega_{12}$ and

(ii)
$$C = \sum_{\underline{b},\underline{b}'} \frac{\langle 0;2\Gamma_{12}^-;\eta_\ell-1;\eta_s+1|H_{ER}(\omega_s)|\underline{b}';2\Gamma_{12}^-;\eta_\ell-1;\eta_s\rangle}{\omega_{\underline{b}'} + 2\omega_{12} - \omega_\ell} \times$$
$$\times \frac{\langle \underline{b}';2\Gamma_{12}^-;\eta_\ell-1;\eta_s|H_{EL}|1s;\Gamma_{12}^-;\eta_\ell-1;\eta_s\rangle\langle 1s;\Gamma_{12}^-;\eta_\ell-1;\eta_s|H_{EL}|\underline{b};0;\eta_\ell-1;\eta_s\rangle}{\omega_{\underline{b}} - \omega_\ell} \times$$
$$\times \langle \underline{b};0;\eta_\ell-1;\eta_s|H_{ER}(\omega_\ell)|0;0;\eta_\ell;\eta_s\rangle \qquad (7)$$

is independent of q. Assumption (i) is based on the theoretical phonon dispersion curves of Carabatos and Prevot.[12] Assumption (ii) was found to be valid in the analysis of the absorption data.[9]

Under these assumptions $R_{2\Gamma_{12}^-}(\omega_\ell)$ reduces to

$$R_{2\Gamma_{12}^-}(\omega_\ell) \sim |C|^2 \sum_{\vec{q}} \left|\frac{1}{\omega_1^0 + (\hbar q^2/2M) + \omega_{12} - \omega_\ell}\right|^2 \qquad (8)$$

$$= 4\pi|C|^2 (2M/\hbar)^{3/2} \int_0^{x_c} \frac{x^{1/2}dx}{|\omega_1^0 + \omega_{12} - \omega_\ell + x|^2} \qquad (9)$$

where $x = \hbar q^2/2M$ and x_c correspond to the Brillouin zone cut-off q_c. The integral in Eq. (9) diverges at the pole $\omega_\ell = (\omega_1^0+\omega_{12})$ when $\omega_\ell \geq \omega_1^0+\omega_{12}$. As pointed out in Section I this difficulty can be avoided by introducing a damping constant γ_1 (if the phonon damping is negligible, γ_1 would be the exciton damping) and writing Eq. (9) as

$$R_{2\Gamma_{12}^{-}}(\omega_\ell) \sim 4\pi|C|^2(2M/\hbar)^{3/2}\int_0^{x_c}\frac{x^{1/2}dx}{(x-x_o)^2+\gamma_1^2(x)} \tag{10}$$

where $x_o = \omega_\ell-(\omega_1^0+\omega_{12})$. We have so far assumed the most general case of γ_1 as function of the momentum $\hbar q$. But then Eq. (10) cannot be integrated unless $\gamma_1(x)$ is known. However, if $\gamma_1(x)$ is small (and from absorption measurements at 4.2°K the 1s exciton damping is known to be $\sim$0.4 cm^{-1} [24]) because of the relation:[17]

$$\lim_{\gamma_1\to 0}\frac{\gamma_1}{(x-x_o)^2+\gamma_1^2} = \pi\delta(x-x_o) \tag{11}$$

We can make the approximation

$$\int_0^{x_c}\frac{x^{1/2}dx}{(x-x_o)^2+\gamma_1^2(x)} \approx \frac{1}{\gamma_1(x_o)}\int_0^{x_c}x^{1/2}\frac{\gamma_1(x)dx}{(x-x_o)^2+\gamma_1(x)} \tag{12}$$

$$= \frac{1}{\gamma_1(x_o)}\int_0^{x_c}x^{1/2}\,\mathrm{Im}\left(\frac{1}{x-x_o-i\,\gamma_1(x)}\right)dx$$

$$\propto \frac{\alpha(x_o)}{\gamma_1(x_o)} \quad (x_o \geq 0) \tag{13}$$

where α is the absorption coefficient of Cu_2O. Substituting Eq. (13) into Eq. (10) we arrived at the simple result that

$$R_{2\Gamma_{12}^{-}}(\omega_\ell) \sim \frac{\alpha(\omega_\ell)}{\gamma_1(\omega_\ell-(\omega_1^0+\omega_{12}))} \quad (\omega_\ell \geq \omega_1^0+\omega_{12}) \tag{14}$$

To bring out the dependence of γ_1 on ω_ℓ we have purposely written γ_1 as $\gamma_1(\omega_\ell-(\omega_1^0+\omega_{12}))$. But one should note that γ_1 is really a function of the momentum $\hbar q$.

The approximation we made in obtaining Eq. (13) is equivalent to saying that $R_{2\Gamma_{12}^-}$ is dominated by scattering processes in which the incident photon ω_ℓ excites an 1s exciton $\omega_1(\vec{q})$ with simultaneous emission of a $\Gamma_{12}^-(-\vec{q})$ phonon so that

$$\omega_\ell = \omega_1^0 + (\hbar q^2/2M) + \omega_{12} \tag{15}$$

Thus the incident photon selects the wave vector q of the two Γ_{12}^- phonons whose Raman cross-section will be enhanced through the resonance conditions (Eq. (15)). Some of the consequences of this special property of RRS in Cu_2O will be shown later on.

Klein[25] has pointed out that Eq. (14) can be written as

$$R_{2\Gamma_{12}^-}(\omega_\ell) \sim \alpha(\omega_\ell)\ \gamma_{rad}/\gamma_1. \tag{16}$$

with $2\pi/\gamma_1$ being identified as the total lifetime of the 1s yellow exciton and $2\pi/\gamma_{rad}$ as the radiative recombination of the exciton with emission of a Γ_{12}^- phonon. Equation (16) was derived by considering the two-phonon scattering process as a two-step 'hot luminescence' process of (1) a Γ_{12}^- phonon-assisted photoexcitation of the 1s exciton, and followed by (2) a Γ_{12}^- phonon-assisted radiative recombination of the exciton. Shen[26] has however shown that Eq. (14) actually has contributions from both RRS and hot luminescence (HL). In the rest of this paper we shall assume γ_1 is always dominated by the exciton damping and use the form of Eq. (16) to study RRS of other multi-phonon modes of Cu_2O.

By making use of Eq. (11), we find that $\alpha \sim [\omega_\ell - (\omega_1^0 + \omega_{12})]^{1/2}$ and Eq. (14) becomes:

$$R_{2\Gamma_{12}^-}(\omega_\ell) \propto \begin{cases} [\omega_\ell - (\omega_1^0+\omega_{12})]^{1/2}\ \gamma_1^{-1} & (\omega_\ell \geq \omega_1^0 + \omega_{12}) \\ 0 & (\omega_\ell < \omega_1^0 + \omega_{12}) \end{cases} \tag{17}$$

This is the expression which was derived in Ref. 4. If γ_1 were constant Eq. (17) would predict that the $2\Gamma_{12}^{-}$ Raman mode should increase above the absorption edge like the absorption coefficient. Figure 5 shows that indeed the $2\Gamma_{12}^{-}$ mode is strongly enhanced at the absorption edge $\omega_1^0+\omega_{12}$ but above the absorption edge the Raman cross-section decreases instead of increasing monotonically like the absorption. This difference in behavior between the Raman cross-section and the absorption has been attributed to a strong dependence of γ_1 on ω_ℓ.[4]

To calculate the momentum dependence of γ_1 we have to consider all the decay mechanisms of the 1s exciton. Some of the decay mechanisms, like scattering by impurities, dislocations or surface and Auger processes, cannot be calculated easily. We have therefore assumed that their contribution to γ_1 is a constant equal to γ_d. The other principal decay mechanisms for the 1s yellow exciton are

(a) radiative recombination;

(b) emission of one phonon;

and (c) emission of two phonons;

These processes are shown diagrammatically in Figure 9(c), (d) and (e).

(a) Radiative Recombination

Since the 1s yellow exciton cannot decay radiatively to the ground state by electric dipole transition, the radiative recombination can only proceed via an electric quadrupole or magnetic dipole or phonon-assisted electric dipole transition. The contributions to γ_1 due to these radiative decay mechanisms are small and can be written as:

Electric Quadrupole or Magnetic Dipole Transitions

$$\gamma_1^{EQ,M} = \left(\frac{2\pi}{\hbar}\right) \left| \langle 0; \eta_s + 1 | H_{ER}^{EQ,M} | 1s; \eta_s \rangle \right|^2 \frac{d\eta_s}{d(\hbar\omega_s)} \tag{18}$$

Γ_{12}^- phonon-assisted Dipole Transition

$$\gamma_{rad} = \left(\frac{2\pi}{\hbar}\right) \left| \sum_{b'} \frac{\langle 1s; 0; \eta_s | H_{EL} | b'; \Gamma_{12}^-; \eta_s \rangle}{\hbar(\omega_b' - \omega_1(\bar{q}) - \omega_{12})} \times \right.$$

$$\left. \times \langle b'; \Gamma_{12}^-; \eta_s | H_{ER} | 0; \Gamma_{12}^-; \eta_s + 1 \rangle \right|^2 \frac{d\eta_s}{d(\hbar\omega_s)} \tag{19}$$

where $H_{ER}^{EQ,M}$ stands for the electric quadrupole or magnetic dipole transition Hamiltonian and $\frac{d\eta_s}{d\omega_s}$ is the scattered photon density of states. $\gamma_1^{EQ,M}$ and γ_{rad} are essentially independent of ω_ℓ and furthermore $\gamma_d + \gamma_\alpha + \gamma_{rad} = \gamma_1(0)$. From the observed external quantum yield of the photoluminescence, it appears $\gamma_d >> \gamma_1^{EQ,M} + \gamma_{rad}$.

(b) One-Phonon Emission

Alternately the 1s exciton can also be scattered by one phonon to another exciton band (interband scattering) or to another state of the 1s exciton band (intraband scattering). Since energy has to be conserved in these real transitions and the 1s band is well separated from other exciton bands we expect the intraband term to dominate over the interband terms.

It is well-known that excitons are more likely to be scattered by longitudinal optical (LO) and longitudinal acoustic (LA) phonons.[27] In Reference 4 it was proposed that the intraband one-phonon scattering of the 1s yellow exciton is due mainly to the LA phonons. In Reference 6 we have provided experimental evidence in support of this proposal (see also Section IV (2)). Applying perturbation theory to Figure 9(d) we can calculate the

contribution to γ_1 due to emission of one LA phonons:

$$\gamma_{ac} = \frac{2\pi}{\hbar} \sum_{\vec{q}_1} | \langle 1s(\vec{q}-\vec{q}_1); LA(\vec{q}_1) | H_{EL}^{LA} | 1s(\vec{q}); 0 \rangle |^2 \delta(\frac{\hbar^2}{2M} [|\vec{q}|^2 - |\vec{q}-\vec{q}_1|^2] - vq_1\hbar) \tag{20}$$

In obtaining Eq. (20) we have assumed that the LA phonon dispersion is isotropic and is given by $\omega_{ac} = vq$ where v is the LA phonon velocity. It was shown in Reference 12 that this is true for q out to approximately one half of the Brillouin zone. The 1s exciton-LA phonon coupling matrix element is given by[27]:

$$\langle 1s(\vec{q}-\vec{q}_1); LA(\vec{q}_1) | H_{EL}^{LA} | 1s(\vec{q}); 0 \rangle = \sqrt{\frac{2\hbar}{9NM'}} (1 + \eta_{q_1}) q_1^{1/2} \times$$

$$\times \{-q_h(\vec{q}_1; 1s; 1s) C_v + q_e(\vec{q}_1; 1s; 1s) C_c\} \tag{21}$$

where C_v, C_c = LA phonon deformation potentials of the valence and conduction bands respectively.

N = number of atoms in the crystal;

$(M')^{-1}$ = 2(mass of oxygen atom)$^{-1}$ + 4 (mass of copper atom)$^{-1}$;

n_{q_1} = $\exp(\hbar v\, q_1/kT) - 1)^{-1} \ll 1$ (since $T \lesssim 10°K$)

= occupation number of the LA phonon;

$q_e(q_1; 1s; 1s) = \{1 + (\frac{m_h a_o q_1}{2(m_e + m_h)})^2\}^{-2}$;

$q_h(q_1; 1s; 1s) = \{1 + (\frac{m_e a_o q_1}{2(m_e + m_h)})^2\}^{-2}$;

m_e, m_h = effective mass of electron and hole respectively;

and a_o = Bohr radius of the 1s exciton.

From the binding energy of the 1s exciton we estimated a_o to be ~ 7 Å. The size of the Brillouin zone is $q_{BZ} \sim 7\times10^7$ cm^{-1}. For $q_1 \lesssim 0.2\, q_{BZ}$ we find $q_1 a_o \lesssim 1$ so the q_1 dependent terms in q_e and q_h can be neglected and we can approximate $q_e = q_h = 1$. This simplifies Eq. (21) to

$$\langle 1s(\vec{q}-\vec{q}_1); LA(\vec{q}_1)|H_{EL}^{LA}|1s(\vec{q}); 0\rangle = g\sqrt{q_1} \tag{22}$$

with $g = (2\hbar/9NM')^{1/2}(C_c - C_v)$

Substituting Eq. (22) into Eq. (20) the summation over q_1 can be carried out to give:

$$\gamma_{ac}(q) = \begin{cases} \dfrac{4V_o g^2 M}{3\pi\hbar^2 q}\left(q - \dfrac{Mv}{\hbar}\right)^3 & \left(q > \dfrac{Mv}{\hbar}\right) \\ 0 & \left(q < \dfrac{Mv}{\hbar}\right) \end{cases} \tag{23}$$

where V_o is the volume of the crystal. Assuming $v=5.15 \times 10^5$ cm/sec[28] and $M \sim 3m_o$ (m_o is the mass of electron)[6] we find $Mv^2 \lesssim 0.24\ cm^{-1} << \hbar vq$. Hence for small $q(\lesssim 0.2\ q_{B.Z.})$ we can approximate Eq. (23) by

$$\gamma_{ac}(q) \sim q^2 \tag{24}$$

(c) Emission of two Γ_{12}^- Phonons

In Figure 5 the $2\Gamma_{12}^-$ mode Raman cross-section shows an abrupt decrease at $\omega_\ell = \omega_1^0 + 3\omega_{12}$. This suggests that there is a significant increase in γ_1 due to intraband scattering of the 1s exciton with emission of $2\Gamma_{12}^-$ phonons which becomes possible when $\omega_1(q) > \omega_1^0 + 2\omega_{12}$. Applying perturbation theory to Figure 9(e) we obtain:

$$\gamma_{2\Gamma_{12}^-}(q) = \frac{2\pi}{\hbar^2}\sum_{\vec{q}_4}\Big|\sum_{\underline{b},\vec{q}_3}\frac{\langle 1s(\vec{q}_4); 2\Gamma_{12}^-|H_{EL}(\Gamma_{12}^-)|\underline{b}(\vec{q}_3); \Gamma_{12}^-\rangle}{\hbar(\omega_{\underline{b}}(\vec{q}_3) - \omega_1(\vec{q}) + \omega_{12})} \times$$

$$\langle \underline{b}(\vec{q}_3); \Gamma_{12}^-|H_{EL}(\Gamma_{12}^-)|1s(\vec{q}); 0\rangle\Big|^2 \delta\left(\frac{\hbar}{2M}(q_4^2 - q^2) + 2\omega_{12}\right) \tag{25}$$

which can be approximated by

$$\gamma_{2\Gamma_{12}^-}(q) \propto \sum_{\vec{q}_4}\delta\left(\frac{\hbar}{2M}(q_4^2 - q^2) + 2\omega_{12}\right)$$

$$\sim \begin{cases} \left(\dfrac{\hbar}{2M}q^2 - 2\omega_{12}\right)^{1/2} & \left(\dfrac{\hbar q^2}{2M} > 2\omega_{12}\right) \\ 0 & \text{otherwise} \end{cases} \tag{26}$$

After summing all the contributions to γ_1 we obtain

$$\gamma_1(q) = \gamma_1(0) + \gamma_{ac}(q) + \gamma_{2\Gamma_{12}^-}(q)$$

Since $\gamma_1(0)$, γ_{ac} and $\gamma_{2\Gamma_{12}^-}$ all contain unknown exciton-phonon matrix elements, it is not possible to calculate them absolutely. Instead we treat their relative magnitudes as adjustable parameters. Making use of Eq. (15) to express q in terms of ω_ℓ, we arrive at the following expression for $R_{2\Gamma_{12}^-}(\omega_\ell)$ from Eq. (17):

$$R_{2\Gamma_{12}^-}(\omega_\ell) \sim \begin{cases} \dfrac{[\omega_\ell - (\omega_1^0 + \omega_{12})]^{1/2}}{A + [\omega_\ell - (\omega_1^0 + \omega_{12})] + B[\omega_\ell - (\omega_1^0 + 3\omega_{12})]^{1/2}} & (\omega_\ell \geq \omega_1^0 + 3\omega_{12}) \\ \dfrac{[\omega_\ell - (\omega_1^0 + \omega_{12})]^{1/2}}{A + [\omega_\ell - (\omega_1^0 + \omega_{12})]} & (\omega_1^0 + \omega_{12} \leq \omega_\ell \leq \omega_1^0 + 3\omega_{12}) \\ 0 & (\omega_\ell < \omega_1^0 + \omega_{12}) \end{cases}$$

The broken line in Figure 5 is a plot of Eq. (27) with $\hbar A$ = 4.8 meV and $\hbar B$ = 3.8 $meV^{1/2}$ (or 39 cm^{-1} and 30 $cm^{-1/2}$ respectively). The fit is quite satisfactory except for $\omega_\ell > \omega_1^0 + 3\omega_{12}$ where the experimental cross-section drops below the theoretical value. The reason for this discrepancy is that, at large ω_ℓ, γ_1 will have contribution from other multiphonon scattering not considered here. This cause the experimental cross-section to decrease faster than the calculated curve.

We therefore conclude that the sharpness of the rise in $R_{2\Gamma_{12}^-}$ at $\omega_\ell \simeq \omega_1^0 + \omega_{12}$ is due to the strong resonance enhancement at the 1s exciton and the decrease in $R_{2\Gamma_{12}^-}$ above the absorption edge is due to γ_1 increasing

faster than the absorption coefficient.

We can now discuss the RRS of the other two-phonon modes based on what we have learned from the $2\Gamma_{12}^-$ mode. All the two-phonon modes showing enhancement in Figure 6 are of the form $\Gamma_{12}^- + P$ (where P is a Γ_{25}^-, Γ_{12}^-, Γ_2^-, $\Gamma_{15}^{-(1)}$ or $\Gamma_{15}^{-(2)}$ phonon). These two-phonon modes have stronger enhancements than other two-phonon modes because the Γ_{12}^- phonon has the strongest coupling between the 1s exciton and exciton $\underline{b}$. When P is different from the Γ_{12}^- phonon we can permute the order in which these two phonons are scattered (see Figure 9(b)). Based on Eq. (14) we should then observe two enhancements in the Raman cross-section corresponding to excitation of the 1s exciton with emission of a Γ_{12}^- phonon or a P phonon. Furthermore these enhancement steps should occur respectively at $\omega_1^0+\omega_{12}$ and $\omega_1^0+\omega_P$. That this is indeed the case is best seen in the $\Gamma_{12}^-+\Gamma_{25}^-$ mode (see Fig. 6).

Let us consider the $\Gamma_{12}^-+\Gamma_{25}^-$ mode in more detail. For $\omega_1^0+\omega_{25}<\omega_\ell<\omega_1^0+\omega_{12}$ only the Γ_{25}^- phonon can be involved in the excitation of the 1s exciton so only the first diagram in Figure 9(b) (with $X = \Gamma_{25}^-$ and $Y = \Gamma_{12}^-$) can contribute to the RRS. When $\omega_\ell > \omega_1^0+\omega_{12}$ both phonons can assist in the absorption of ω_ℓ so that the two diagrams in Figure 9(b) have to <u>summed first and then squared</u> to give

$$R_{\Gamma_{12}^-+\Gamma_{25}^-}(\omega_\ell) \sim \sum_q \left| \frac{A}{\omega_1^0+\hbar q^2/2M+\omega_{12}(\vec{q})-\omega_\ell} + \frac{B}{\omega_1^0+\hbar q^2/2M+\omega_{25}(-\vec{q})-\omega_\ell} \right|^2 \quad (28)$$

where the coefficient A and B are assumed to be independent of $\vec{q}$.

One can show easily that $|A|^2 = |B|^2$. It is now possible for the two terms in Eq. (28) to interfere with each other. In case of the $\Gamma_{12}^- + \Gamma_{25}^-$ mode we found that these two terms do not interfere. The reason is that the two terms in Eq. (28) have different denominators and hence for a given ω_ℓ and q at most one of the two terms is at resonance. When one term is at resonance the other non-resonsnt term is negligible (this is true because the ls exciton damping is small compared to $\omega_{12}-\omega_{25}$). Under such circumstances we can rewrite Eq. (28) as

$$\overset{R}{\Gamma_{12}^- + \Gamma_{25}^-}(\omega_\ell > \omega_1 + \omega_{12}) \sim \sum_q \left\{ \left| \frac{A}{\omega_1^0 + \hbar q^2/2M + \omega_{25} - \omega_\ell} \right|^2 + \left| \frac{B}{\omega_1^0 + \hbar q^2/2M + \omega_{12} - \omega_\ell} \right|^2 \right\} \tag{29}$$

We note that for $\omega_\ell < \omega_1^0 + \omega_{12}$ only the first term in Eq. (29) contribute to the $\Gamma_{12}^- + \Gamma_{25}^-$ cross-section. Thus according to Eq. (29) the Raman cross-section of the $\Gamma_{12}^- + \Gamma_{25}^-$ mode should show two approximately equal enhancement steps one at $\omega_1 + \omega_{25}$ and the other at $\omega_1 + \omega_{12}$. This is indeed what is observed experimentally as shown in Figure 6.

We have pointed out that one special feature of the RRS of the $2\Gamma_{12}^-$ mode in Cu_2O is that the incident photon selects the wave vector of the incident phonon through the resonance condition (Eq. (15)). If we assume the Γ_{12}^- phonon dispersion is isotropic, from the Raman spectrum we can measure $2\omega_{12}(q)$. Substituting $\omega_{12}(q)$ into Eq. (15) we can obtain q if M is known. Thus theoretically we can deduce the phonon dispersion curve of the Γ_{12}^- mode by RRS. The magnitude of q one can observe in this way

depends on M, and ω_ℓ and on whether the Raman mode is observable. For example if we substitute $M = 3\ m_o$, $\hbar\omega_1^0 = 2.033$ eV, $\hbar\omega_{12} = 13.6$ meV and $\hbar\omega_\ell = 2.15$ eV into Eq. (15) we find $q = 2.85\times10^7\ cm^{-1} \sim 0.4\ q_{B.Z.}$.

We have observed no change in the energy of the $2\Gamma_{12}^-$ mode for $\hbar\omega_\ell$ out to 2.15 eV so the Γ_{12}^- mode has essentially no dispersion out to $q \sim 0.4\ q_{B.Z.}$. Examining the other two-phonon modes in Figure 7 we conclude that the Γ_{25}^- phonon shows very little dispersion also. The $\Gamma_{12}^- + \Gamma_{15}^{-(1)}$ modes show a splitting with increase in ω_ℓ. We interpret this splitting as due to an increase in the $\Gamma_{15}^{-(1)}$(LO) phonon energy with q. The zone-center TO-LO splitting of the $\Gamma_{15}^{-(1)}$ phonon is $2\ cm^{-1}$ from Table 1. Our spectrometer slit width is $\sim 5\ cm^{-1}$ so that for $\omega_\ell \sim \omega_1^0+\omega_{12}$ it is not possible to resolve the $\Gamma_{12}^- + \Gamma^{-(1)}_{15}$(TO) peak from the $\Gamma_{12}^- + \Gamma_{15}^{-(1)}$(LO) peak. When ω_ℓ is increased, the $\Gamma^{-(1)}_{15}$(LO) phonon energy increases linearly (or quadratically with q) while the $\Gamma_{15}^{-(1)}$(TO) phonon energy changes little. As a result the $\Gamma_{12}^- + \Gamma_{15}^{-(1)}$(LO) Raman peak splits off from the $\Gamma_{12}^- + \Gamma_{15}^{-(1)}$(TO) peak in Figure 8. At $\omega_\ell/2\pi c = 16\ 864\ cm^{-1}$ (corresponding to $q \sim 1/4\ q_{B.Z.}$) this splitting becomes as large as $8\ cm^{-1}$. These results deduced from RRS of Cu_2O agree well with the phonon dispersion curves of Cu_2O calculated by Carabatos and Prevot.[12] Their calculated phonon dispersion curves for the Γ_{12}^-, Γ_{25}^- and $\Gamma_{15}^{(1)}$(TO) phonon indeed show little dispersion while the $\Gamma_{15}^{-(1)}$(LO) phonon increases in energy as q^2 near $q \sim 0$. Furthermore based on their result we estimate that the TO-LO splitting of the $\Gamma_{15}^{-(1)}$ phonon would be $\sim 9\ cm^{-1}$ at $\omega_\ell/2\pi c = 16\ 864\ cm^{-1}$.

(2) RRS of Three-phonon Modes of Cu_2O: $2\Gamma_{12}^-$ + P (where P is a LA, Ta, Γ_{12}^-, Γ_{25}^- or $\Gamma_{15}^{-(1)}$ Phonon)

The peaks labelled as X, Y and Z in Figure 7 shift more appreciably in frequencies with ω_ℓ than the $\Gamma_{12}^- + \Gamma_{15}^{-(1)}$ modes. That these peaks approach the $2\Gamma_{12}^-$ mode as ω_ℓ approaches $\omega_1^0+\omega_{12}$ suggests that they arise from multiphonon scattering of two Γ_{12}^- phonons and a dispersive excitation. Furthermore these excitations have probably a linear dispersion since X, Y and Z seem to shift with $(\omega_\ell-\omega_1^0-\omega_{12})^{1/2}$ (and hence linearly with q). We have identified these dispersive excitations as acoustic phonons and X, Y, and Z respectively as $2\Gamma_{12}^-$ + TA, $2\Gamma_{12}^-$ + LA and $2\Gamma_{12}^-$ + 2LA modes. These identifications are supported by the quantitative analysis of their line-shapes, and the ω_ℓ dependence of their peak energies and Raman cross-sections. The peak Z, identified as a four-phonon mode, will be considered later together with other four-phonon modes. We will consider the peak Y first as a three-phonon mode of Cu_2O.

$2\Gamma_{12}^-$ + LA Mode

We first calculate the Raman cross-section for the three-phonon scattering process shown in Figure 9(f). Using perturbation theory and derivations analogous to that of Eq. (9) we can show that

$$R_{2\Gamma_{12}^-+\omega_{ac}(\vec{k})} \propto \sum_{\vec{q}} \left| \sum_{\underline{b}'} \frac{\langle \underline{b}';\Gamma_{12}^-+LA;n_\ell-1;n_s|H_{EL}(LA)|1s(\vec{q});\Gamma_{12}^-;n_\ell-1;n_s\rangle}{(\omega_1^0+\hbar q^2/2M+\omega_{12}-\omega_\ell+i\gamma_1)(\omega_{b'}+\omega_{ac}(\vec{k})+\omega_{12}-\omega_\ell-i\gamma_{b'})}\right|^2$$

where $\vec{k}$ and ω_{ac} are the wave vector and frequency of the LA phonon emitted. Of all the possible intermediate states $\underline{b}'$ again only the 1s yellow exciton state $\omega_1(\vec{q}-\vec{k})$ is resonant so we can rewrite Eq. (30) as:

$$R_{2\Gamma_{12}^- + \omega_{ac}(R)} \propto \sum_{\vec{q}} \left| \omega_1^0 + \frac{\hbar q^2}{2M} + \omega_{12} - \omega_\ell - i\gamma_1(q) \right|^{-2} \times$$

$$\times \left| \frac{\langle \underline{b}'; \Gamma_{12}^- + LA; n_\ell - 1; n_s | H_{EL}(LA) | 1s(\vec{q}); \Gamma_{12}^-; n_\ell - 1; n_s \rangle}{\omega_1^0 + \frac{\hbar}{2M} |\vec{q} - \vec{k}|^2 + vk + \omega_{12} - \omega_\ell - i\gamma_1(|\vec{q} - \vec{k}|)} \right|^2 \qquad (31)$$

Using Eq. (12), Eq. (31) can be simplified into:

$$R_{2\Gamma_{12}^- + \omega_{ac}(\vec{k})} \propto \sum_{\vec{q}} \gamma_1^{-1}(q) \delta(\omega_1 + \frac{\hbar q^2}{2M} + \omega_{12} - \omega_\ell)\ \gamma_1^{-1}(|\vec{q} - \vec{k}|)\ \delta(\frac{\hbar}{2M}[|\vec{q} - \vec{k}|^2 - q^2] + vk) \times$$

$$\times \left| \langle 1s(\vec{q} - \vec{k}); \Gamma_{12}^- + LA | H_{EL}(LA) | 1s(\vec{q}); \Gamma_{12}^- \rangle \right|^2 \qquad (32)$$

The total $R_{2\Gamma_{12}^- + LA}$ at a given ω_s is obtained by summing Eq. (32) over $\vec{k}$ satisfying $2\omega_{12} + \omega_{ac}(\vec{k}) = \omega_\ell - \omega_s$. Since the LA phonon velocity v is assumed to be isotropic, we have to sum over all orientations of $\vec{k}$. The delta-function $\delta(\frac{\hbar}{2M}[|\vec{q} - \vec{k}|^2 - q^2] + vk)$ restricts the values of k to those satisfying the condition:

$$q - \frac{2Mv}{\hbar} \leq |\vec{q} - \vec{k}| \leq q \text{ or equivalently } 0 \leq k \leq 2(q - \frac{Mv}{\hbar}) \qquad (33)$$

As shown before, except for very small q, $Mv/\hbar \ll q$ so we can approximate $\gamma_1(|\vec{q} - \vec{k}|)$ in Eq. (32) by $\gamma_1(q)$. This simplification allows us to express the Raman cross-section of the $2\Gamma_{12}^- + LA$ mode as

$$R_{2\Gamma_{12}^- + LA}(\omega_\ell, \omega_s = \omega_\ell - 2\omega_{12} - vk) = \begin{cases} \alpha(\omega_\ell)\ \gamma_{rad}\ \gamma_{ac}(q,k)\gamma_1^{-2}(q) & \text{for } 0 \leq k \leq 2(q - \frac{Mv}{\hbar}) \\ 0 & \text{otherwise} \end{cases} \qquad (34)$$

where $\gamma_{ac}(q,k)$ is defined as

$$\gamma_{ac}(q,k) = \frac{2\pi}{\hbar^2} \int d\Omega_k \left| \langle 1s(|\vec{q}-\vec{k}|);\ LA(\vec{k}) | H_{EL}(LA) | 1s(q);0 \rangle \right|^2 \times$$

$$\times\ \delta\left(\frac{\hbar}{2M}\left[q^2 - |\vec{q}-\vec{k}|^2\right] - vk\right) \qquad (35)$$

($\int d\Omega_k$ is over all orientations of $\vec{k}$). Physically, $\gamma_{ac}(q,k)$ is the probability of the 1s exciton being scattered by LA phonons of frequency $\omega_{ac}(k)$ and is related to $\gamma_{ac}(q)$ defined in Eq. (20) by

$$\gamma_{ac}(q) = \sum_k \gamma_{ac}(q,k) \ .$$

The physical meaning of Eq. (34) is obvious: The incident photon excites a 1s exciton with emission of a Γ_{12}^- phonon. As discussed earlier in Sec. IV(1), the exciton can decay by emission of an LA phonon into a lower exciton state which radiatively recombines with emission of another Γ_{12}^- phonon. This gives rise to a $2\Gamma_{12}^-$ + LA mode in the Raman spectrum. The probability for a 1s exciton of momentum $\hbar q$ to emit a LA phonon $\omega_{ac}(k)$ is given by $\gamma_{ac}(q,k)\gamma_{1s}^{-1}(a)$; so Eq. (34) is simply obtained by multiplying Eq. (16) by this additional term. The scattering of the 1s exciton by the LA phonon considered here is very analogous to the 'cascade' process proposed by Martin and Varma[29] to explain the multi-LO phonon RRS in CdS.

If k is assumed to be small as in Eq. (24) we find that

$$\gamma_{ac}(q,k) \sim k^2 q^{-1} \ . \qquad (36)$$

Substituting this result into Eq. (34) we obtain the Raman lineshape of the $2\Gamma_{12}^-$ + LA mode as

$$I_{2\Gamma_{12}^- + LA}(\delta\omega = \omega_L - \omega_S - 2\omega_{12}) \propto (\delta\omega)^2 \text{ for } 0 \leq \delta\omega \leq 2v(q - Mv/\hbar) \qquad (37)$$

8 and we note that the agreement between theory and experiment is very good. It is now easy to understand why the peak position of Y varies roughly as $(\omega_\ell-(\omega_1^0+\omega_{12}))^{1/2}$. If we neglect the broadening due to the slit function and use Eq. (37), Y should have a sharp peak at $\delta\omega_{max} = 2v(q-Mv/\hbar)\simeq 2qv$. By virtue of Eq. (15), $\delta\omega_{max} \sim (\omega_\ell-(\omega_1^0+\omega_{12}))^{1/2}$.

The effective masses of the conduction and valence band (m_e and m_h) forming the yellow exciton have been measured by Zhilich et al.[30] using magneto-absorption. If the effective mass approximation is valid for the 1s yellow exciton, we would obtain from Zhilich et al.'s result $M = m_e + m_h = 1.45\ m_o$. This value of M is smaller than the value we deduced from RRS by roughly a factor of two and suggests that the effective mass approximation is not valid for the 1s yellow exciton. This is not surprising considering the fact that the observed position of the 1s exciton is off from the value predicted by Eq. (1) by more than 300 cm^{-1}. In the Appendix we shall show that central-cell correction can qualitatively explain this larger value of M for the 1s exciton.

As a further check on our theory we have plotted the peak Raman cross-section of Y as a function of ω_ℓ in Figure 11. The solid curve is obtained from Eq. (34) by putting $k = 2(q-Mv/\hbar)$ and $\gamma_1 = A+(\omega_\ell^0-(\omega_1+\omega_{12})) + B[(\omega_\ell-(\omega_1^0+3\omega_{12})]^{1/2}$ as we did for $R_{2\Gamma_{12}^-}$. The data were fitted by using $A = 45\ cm^{-1}$ and $B \simeq 20\ cm^{1/2}$, in reasonable agreement with the values $A = 39\ cm^{-1}$ and $B = 30\ cm^{-1/2}$ obtained from $R_{2\Gamma_{12}^-}$. If we sum Eq. (34) over all values of k we should obtain R_Y, the total cross-section of Y. It

To compare Eq. (37) with the experimental lineshape it is necessary to convolute Eq. (37) with the spectrometer slit function which is a Gaussian $\exp[-(\omega/\Delta)^2]$ with $\Delta \simeq 3\ cm^{-1}$. This gives the Raman spectrum as

$$I_{2\Gamma_{12}^{-}+LA}(\delta\omega) \propto \int_0^{2v(q-Mv/\hbar)} d\omega' (\omega')^2 \exp\{-[(\omega'-\delta\omega)/\Delta]^2\} \qquad (38)$$

In Figure 10 we have fitted the lineshape of the peak Y for several ω_ℓ's with Eq. (38) treating M as an adjustable parameter. In each case the peak height of the theoretical curve is normalized to the experimental value. For most ω_ℓ the peak Y overlaps with the luminescence or other Raman peaks resulting in some uncertainty in its low energy tail. This partly accounts for why the experimental curves are sharper than the calculated ones. Part of the discrepancy can be due to the approximation we made in the exciton-LA phonon matrix element (Eq. (22)). This is supported by the fact that the discrepancy is smaller for ω_ℓ close to $\omega_1^0 + \omega_{12}$ (where the condition $q \lesssim 0.2 q_{B.Z.}$ is satisfied). Presumably the agreement between theory and experiment can be improved if the correct expression (Eq. (21)) is used but this will introduce more unknown parameters (such as C_c and C_v).

The values of M used to fit the experimental spectra were found to be fairly constant with $M = (3.0 \pm 0.2)\ m_o$. Using this value of M we can calculate numerically from Eq. (38) the dependence of the peak position of the $2\Gamma_{12}^{-} + LA$ mode on ω_ℓ. This is shown as the solid line in Figure

can be seen easily that for $\omega_\ell < \omega_1^0 + 3\omega_{12}$

$$\frac{R_Y}{R_{2\Gamma_{12}^-}} = \frac{\gamma_{ac}(q)}{\gamma_1(q)} = \frac{\omega_\ell - (\omega_1^0+\omega_{12})}{A+\omega_\ell-(\omega_1^0+\omega_{12})} \qquad (39)$$

Using $A \tilde{=} 40\ cm^{-1}$ in Eq. (39) we calculate that $R_Y/R_{2\Gamma_{12}^-} = 0.21$, 0.33 and 0.56 for $\omega_\ell/2\pi c = 15620.5$, 16540 and 16560 cm^{-1} respectively. The experimentally measured ratio of R_Y to $R_{2\Gamma_{12}^-}$ at these ω_ℓ's are respectively 0.18, 0.38 and 0.6 in good agreement with theory.

$2\Gamma_{12}^- +$ TA Mode

The similarity in behavior of the peak X to that of Y suggests that it is a $2\Gamma_{12}^-$ + TA mode. It's much weaker intensity prevents us from making quantitative analysis of its lineshape. However, we can analyze the dependence of its peak position on ω_ℓ using Eq. (38). Using $M = 3.0m_o$ and a TA phonon velocity equal to 0.3v we obtain the solid curve in Figure 8. This TA phonon velocity from RRS agrees well with the value 0.32v calculated from the elastic constants of Cu_2O[28]. From the relative magnitude of the $2\Gamma_{12}^-$ + LA and $2\Gamma_{12}^-$ + TA Raman peaks we estimated that

$$\left|\frac{\langle 1s;LA|H_{EL}(LA)|1s;0\rangle}{\langle 1s;TA|H_{EL}(TA)|1s;0\rangle}\right|^2 \tilde{=} 45.$$

To our knowledge this is the first time the relative magnitude of the LA and TA phonons-1s exciton matrix element has been measured directly. This large ratio also supports the proposal in Ref. 4 that the 1s exciton decays predominantly by emission of a LA phonon.

$2\Gamma_{12}^- + F$ ($F = \Gamma_{12}^-$, Γ_{25}^-, and $\Gamma_{15}^{-(1)}$ Mode)

Raman scattering of three odd-parity zone-center phonons in Cu_2O is

forbidden by parity selection rule. The scattering becomes allowed, however, if one or more of the scattered phonons has a finite momentum.[1]

To determine the Raman processes responsible for the enhancements observed in Figure 7 we look for processes which have as many resonant intermediate states as possible. It is not difficult to conclude that there are only three such Raman processes as shown in Figure 9(g). In all three processes there can be two resonant intermediate states. When the phonon P is not a Γ_{12}^- phonon we can further argue that process (i) in Figure 9(g) dominates over the other two. If this were not the case we would expect the $3\Gamma_{12}^-$ mode to be much stronger than the other three phonon modes because the coupling between the 1s exciton and the dipole allowed excitons (represented by ⟹ in Figure 9(g)) is much stronger for the Γ_{12}^- phonon that for the other odd-parity phonons.

The validity of the above arguments can be checked by calculating the Raman cross-section $R_{2\Gamma_{12}^- + P}$ ($P = \Gamma_{12}^-$, Γ_{25}^- or $\Gamma_{15}^{-(1)}$ phonon) for process (i) in Figure 9(g) and comparing the result with experiment. From the simple physical picture of the Raman process as consisting of (a) absorption of incident photon with emission of a Γ_{12}^- phonon and excitation of a 1s exciton; (b) cascading of the 1s exciton down the exciton band with emission of the P phonon and (c) radiative recombination of the exciton with emission of a second Γ_{12}^- phonon we obtain the Raman cross-section as

$$R_{2\Gamma_{12}^- + P}(\omega_\ell) = \begin{cases} \alpha(\omega_\ell)\,\gamma_{rad}\,\gamma_P(q)\gamma_1^{-1}(q)\gamma_1^{-1}(q') & \text{for } \omega_\ell > \omega_1^0 + \omega_{12} + \omega_P \\ 0 & \text{otherwise} \end{cases} \tag{40}$$

where q and q' are the 1s exciton wave vector defined by the conservation of energy in steps (a) and (b):

$$\omega_\ell = \omega_1^0 + \hbar q^2/2M + \omega_{12} \text{ and } \frac{\hbar}{2M}(q^2 - q'^2) = \omega_P.$$

γ_P, the contribution to γ_1 due to emission of one phonon P, is given by:

$$\gamma_P(q) = 2\pi/\hbar^2 \sum_{\vec{k}} |\langle 1s(\vec{q}-\vec{k}); P(\vec{k})|H_{EL}(P)|1s(\vec{q}); 0\rangle|^2 \delta(\frac{\hbar}{2M}(q^2 - |\vec{q}-\vec{k}|^2 - \omega_P) \quad (41)$$

One difference between the acoustic phonons and the odd parity optical phonons is that the 1s exciton-phonon matrix elements for the latter vanish at $k = 0$ due to parity selection rule.

To calculate γ_P it is necessary to know the momentum dependence of the exciton-phonon interaction. Unfortunately this information is not available for the Γ_{12}^- and Γ_{25}^- phonons. Because of the macroscopic electric field associated with the LO phonons we expect the $\Gamma_{15}^{-(1)}$(LO) phonon-1s exciton interaction to be dominated by the Frölich-type interaction.[1,27] Under this assumption the exciton-LO phonon matrix element is given by:

$$\langle 1s(\vec{q}-\vec{k}); \Gamma_{15}^-(\vec{k})|H_{EL}(LO)|1s(\vec{q})\rangle = [\frac{2\pi\hbar e^2}{V_o}(\frac{1}{\epsilon_\infty} - \frac{1}{\epsilon_o})]^{1/2} \times$$

$$\times k^{-1}\{q_e(\vec{k};1s;1s) - q_h(\vec{k};1s;1s)\} \quad (42)$$

where ϵ_o and ϵ_∞ are respectively the static and optical frequency dielectric constants of Cu_2O. The k dependent term in Eq. (42) are q_e and q_h which have been defined in Eq. (21). We have estimated the parameters m_e/m_h and a_o in q_e and q_h in this manner. m_e and m_h have been determined by magneto-absorption,[30] although we have found M

for the 1s yellow exciton different from the value obtained from magneto-absorption, we shall assume the mass ratio m_e/m_h to be the same in both cases (i.e. $m_e/m_h = 0.724$). The 1s exciton radius a_o has not been determined so it is estimated from the equation:

$$a_o = (2\varepsilon \times \text{Binding Energy of the 1s exciton})^{-1} \quad (43)$$

The dielectric constant ε can have any value between $\varepsilon_o(7.4)$ and $\varepsilon_\infty(6.5)$[13] depending on a_o[31] (see Appendix). Here we simply take $\varepsilon \simeq 7$ and obtain $a_o \simeq 7A$. Using these values of a_o, and $A = 40\ cm^{-1}$ we have calculated numerically $R_{2\Gamma_{12}^- + \Gamma_{15}^{-(1)}}$ as a function of ω_ℓ. The result is shown as the solid curve in Figure 7. The agreement with experiment is satisfactory considering that there is no adjustable parameter other than an overall normalization.

It should be noted that $R_{2\Gamma_{12}^- + P}$ is dependent on $\alpha(\omega_\ell)$ like $R_{2\Gamma_{12}^-}$ but $R_{2\Gamma_{12}^- + P}$ does not exhibit a step at $\omega_1^0 + \omega_{12}$. This is because the double-resonance condition in Eq. (40) requires $\omega_\ell > \omega_1^0 + \omega_{12} + \omega_P$ and produces the step at $\omega_1^0 + \omega_{12} + \omega_P$ in $R_{2\Gamma_{12}^- + P}$. The diagram (iii) in Figure 9(g), if effective would produce a step in $R_{2\Gamma_{12}^- + P}$ at $\omega_1^0 + 2\omega_{12}$.

From Eq. (40) we can obtain relative magnitudes of γ_P for P = LA, $\Gamma_{15}^{-(1)}$, Γ_{12}^- or Γ_{25}^- phonon by comparing the relative Raman cross-section of the three-phonon modes $2\Gamma_{12}^- + P$. As an example for $(\omega_\ell/2\pi c) = 16\ 689\ cm^{-1}$ we find $\gamma_{ac} : \gamma_{\Gamma_{25}^-} : \gamma_{\Gamma_{12}^-} : \gamma_{\Gamma_{15}^{-(1)}} = 1 : 0.14 : 0.18 : 0.21$. This shows that although our earlier approximation in neglecting the contributions of $\gamma_{\Gamma_{25}^-}$, $\gamma_{\Gamma_{12}^-}$, and $\gamma_{\Gamma_{15}^-}$ to γ_1 is a reasonable one, a more complete theory should also

include these terms which presumably accounts for some of the discrepancy between theory and experiment in Figure 5.

(3) RRS of Four-phonon Modes of Cu_2O: $2\Gamma_{12}^- + 2LA$ and $4\Gamma_{12}^-$

The 'cascade' processes of the 1s exciton discussed above can in principle continue and give rise to higher order multiphonon scattering. Raman scattering of as many as nine LO phonons has been reported in CdS[32]. The probability for the higher order processes will of course decrease with increase in the number of phonons involved. In Cu_2O we have observed a few four-phonon modes but we will consider only the two stronger ones: one is the peak labelled Z in Figure 8 which has been identified as a $2\Gamma_{12}^- + 2LA$ mode and the other one is a $4\Gamma_{12}^-$ mode.

$2\Gamma_{12}^- + 2LA$ Mode

The Raman cross-section for the scattering of ω_ℓ into $\omega_s=\omega_\ell - (2\omega_{12} + \omega_{ac}(k_1) + \omega_{ac}(k_2))$ can be obtained in the same way as in Eq. (34):

$$R_{2\Gamma_{12}^-+2LA}(\omega_\ell) = \alpha(\omega_\ell)\ \gamma_{rad}\ \gamma_{ac}(q,k_1)\gamma_{ac}(q,k_2)\gamma_1^{-3}(q) \qquad (44)$$

for $\omega_\ell \geq \omega_1^0 + \omega_{12}$, $0 \leq k_1 \leq 2(q-Mv/\hbar)$ and $0 \leq k_2 \leq 2(q^2-2Mvk_1/\hbar)^{1/2}-2Mv/\hbar$ and zero otherwise. These limits on k_1 and k_2 are imposed by the conservation of energy and monentum. The total scattered intensity at ω_s is obtained by summing over all possible combinations of $\omega_{ac}(k_1)$ and $\omega_{ac}(k_2)$ satisfying $\delta\omega = \omega_\ell - \omega_s - 2\omega_{12} = \omega_{ac}(k_1) + \omega_{ac}(k_2)$. Using Eq. (36) the Raman spectrum for a given ω_ℓ is given by:

$$I_{2\Gamma_{12}^-+2LA}(\delta\omega) \sim \int_{\omega'_{min}}^{\omega'_{max}} d\omega'(\omega')^2(\delta\omega-\omega')^2 \qquad (45)$$

with ω_{max} = minimum of $\delta\omega$ and $2v(q-Mv/\hbar)$ and ω_{min} = maximum of 0 and $\delta\omega-2Mv^2/\hbar-2v(q^2-2M\delta\omega/\hbar)^{1/2}$. These limits on ω' are derived from the corresponding limits on k_1 and k_2.

We note that the spectrum represented by Eq. (37) has an abrupt cut-off at $\delta\omega=2v(q-Mv/\hbar)$. This sharp edge is smoothed out by convolution with the spectrometer slit function. However, the spectra represented by Eq. (45) have no sharp edges so Eq. (45) is a good approximation for comparison with experimental lineshapes (see Figure 12).

The peak positions of $I_{2\Gamma_{12}^-+2LA}$ can be calculated numerically as a function of ω_ℓ. This is shown as the solid curve in Figure 8 through the experimental points for Z using $M = 3.0\ m_o$ and no adjustable parameter. The excellent agreement between theory and experiment supports our identification of Z. In Figure 12 we have fitted the lineshape of Z for several ω_ℓ with Eq. (45) normalizing the peak height only. As in the case of the peak Y we find that the experimental curves are sharper than the calculated ones. The discrepancy is worse in this case probably because the exciton - LA phonon matrix element occurs twice in Eq. (44).

$\underline{4\Gamma_{12}^-\ \text{Mode}}$

In Figure 4(c) we can identify a number of high energy Raman lines of Cu_2O as four-phonon modes. These occur at 416 cm^{-1} ($3\Gamma_{12}^- + \Gamma_{25}^-$ mode), 438 cm^{-1} ($4\Gamma_{12}^-$ mode) and 481 cm^{-1} ($3\Gamma_{12}^- + \Gamma_{15}^{-(1)}$ mode). Of these the strongest one is the $4\Gamma_{12}^-$ mode so it will be considered in more detail.

The dispersion of the Raman cross-section of the $4\Gamma_{12}^-$ mode is shown in Figure 7. The fact that the 'on-set' in the Raman cross-section occurs at $\sim$ 16 740 $cm^{-1} = \omega_1^2 + 3\omega_{12}$ suggests that the enhancement is due

to the two scattering processes shown in Figure 9(h). The difference between these two processes is that in 9(h)(i) there is a single cascade process involving two Γ_{12}^- phonons. Of these two diagrams in Figure 9(h) we believe that (i) is dominant from the following arguments.

If process (ii) were dominant the Raman cross-section of the $4\Gamma_{12}^-$ mode would be:

$$R_{4\Gamma_{12}^-}(\omega_\ell) = \alpha(\omega_\ell)\gamma_{rad}\,\gamma_{\Gamma_{12}^-}(q)\gamma_{\Gamma_{12}^-}(q')\gamma_1^{-1}(q)\gamma_1^{-1}(q')\gamma_1^{-1}(q'') \qquad (47)$$
$$(\omega_\ell \geq \omega_1^0 + 3\omega_{12})$$

where q,q' and q" are determined by energy conservation as in Eq. (40). This implies $R_{4\Gamma_{12}^-}/R_{3\Gamma_{12}^-} = \gamma_{\Gamma_{12}^-}/\gamma_1 \tilde{=} 0.2$. Experimentally we found that the $4\Gamma_{12}^-$ mode is comparable in strength to the $3\Gamma_{12}^-$ mode. Similar to Eq. (47) we can write down $R_{3\Gamma_{12}^-+\Gamma_{25}^-}$ and $R_{3\Gamma_{12}^-+\Gamma_{15}^{-(1)}}$. From the relative magnitudes of $\gamma_{\Gamma_{12}^-}$, $\gamma_{\Gamma_{15}^{-(1)}}$ and $\gamma_{\Gamma_{25}^-}$ obtained previously we would conclude all the four-phonon modes: $4\Gamma_{12}^-$, $3\Gamma_{12}^- + \Gamma_{25}^-$ and $3\Gamma_{12}^- + \Gamma_{25}^-$ should be of comparable strength. Experimentally we find the $4\Gamma_{12}^-$ mode much stronger than the other two. This suggests that $R_{2\Gamma_{12}^-}$ is not dominated by scattering process (ii) in Figure 9(h).

If we assume that diagram (i) in Figure 9(h) is the only one contributing to $R_{4\Gamma_{12}^-}$ we would obtain

$$R_{2\Gamma_{12}^-}(\omega_\ell) = \alpha(\omega_\ell)\,\gamma_{rad}\,\gamma_{2\Gamma_{12}^-}(q)\gamma_1^{-1}(q)\gamma_1^{-1}(q') \text{ for } \omega_\ell \geq \omega_1^0+3\omega_{12} \qquad (48)$$

instead of Eq. (47). The relatively strong $R_{4\Gamma_{12}^-}$ observed experimentally is consistent with the fact that $\gamma_{2\Gamma_{12}^-}$ makes a significant contribution to

γ_1 as we have discussed earlier in Section IV(1).

CONCLUSION

We have measured the two-phonon, three-phonon and four-phonon resonant Raman scattering in Cu_2O in the vicinity of the Γ_{12}^- phonon-assisted 1s yellow excitonic absorption edge. In all cases the observed enhancements were attributed to resonance with the 1s yellow exciton. The experimental results are compared with theoretical calculations based on perturbation theory. Good agreement was found between experiment and theory with a dispersive damping constant for the 1s yellow exciton. A simple model was used to calculate this damping constant and was found to be consistent with all our experimental results. We have demonstrated also how resonant Raman scattering can be used to probe phonon dispersion in a crystal. In summary we have found resonance Raman scattering to be a very powerful technique in studying the properties of excitons, phonons and their interaction with each other in crystals such as Cu_2O.

ACKNOWLEDGEMENT

We would like to thank Professors L. Falicov and Y. Petroff for their cooperation in the earlier parts of this project and for numerous discussions. One of the authors (PYY) is grateful to Dr. J. E. Smith, Jr. for the use of the Raman spectrometer, Professor L. J. Sham for helpful discussions on the problem of central-cell correction in the 1s yellow exciton and to Dr. F. Stern for a critical reading of the manuscript. The technical assistance of J. A. Bradley is also acknowledged.

This research was supported in part by the Atomic Energy Commission.

APPENDIX

In this appendix we will discuss the importance of central-cell correction to the 1s yellow exciton in Cu_2O and show how such corrections may account for the larger effective mass M of the 1s yellow exciton as determined from our RRS results.

First we briefly review the results of the hydrogenic model of excitons.[10] In this model the exciton is assumed to be formed from a hole in the valence band and an electron in the conduction band. Both bands are assumed to be parabolic with effective masses m_h and m_e respectively (effective mass approximation). The electron and hole are attracted to each other by a screened Coulomb interaction $-e^2/\varepsilon r$ (where ε is the dielectric constant of the crystal). The energies of the exciton are then given by the well-known solution of the hydrogen atom:

$$\hbar\omega_{\substack{\rightarrow \\ nq}} = \hbar^2 q^2/2M + (\hbar\omega_\infty - Bn^{-2}) \quad n = 1,2,\ldots . \tag{A1}$$

In Eq. (A1) the first term describes the motion of the exciton as a whole (center-of-mass motion) so $\hbar\vec{q}$ is the momentum of the exciton and M is the effective mass of the exciton. Within the effective mass approximation $M = m_e + m_h$. The second term in Eq. (A1) describes the relative motion between the electron and hole and is given by a Rydberg series. The binding energy B of the exciton is given by

$$B = \mu e^4/2\varepsilon^2\hbar^2 \tag{A2}$$

where $\mu = m_e m_h (m_e+m_h)^{-1}$ is the reduced mass. The 'Bohr radius' of the exciton is given by:

$$a_o = \hbar^2\varepsilon/\mu e^2 \qquad \text{(A3)}$$

Although the above model works very well for some materials, it is also well-known that in a number of ionic crystals (e.g. PbI_2[33] and RbI[34]) and solid rare gases (e.g. Kr and Xe[35]) the binding of the 1s exciton ground state deviates from Eq. (A1). In these cases one finds that the experimentally observed energy of the 1s level ($\hbar\omega(1s)$) is different from the energy $\hbar\omega_1$ calculated from Eq. (A1) obtained by fitting the n=2, 3 and high exciton levels. A 'hydrogenic defect' C can be defined as[36]:

$$C = (\omega(1s) - \omega_1)/\omega_1 \qquad \text{(A4)}$$

There are two causes for this deviation from the hydrogenic model. One is related to the dynamic interaction between the exciton and phonon. The second cause is associated with the breakdown of the effective mass approximation used to derive Eq. (A1) due to the cellular structure of the crystal.[36] This breakdown of the effective mass approximation necessitates the central-cell corrections.

The value of C for Cu_2O using Eq. (1) and $\omega(1s)/2\pi c = 16\ 399.5\ cm^{-1}$ is 0.43, as compared to 0.13 and -0.07 for solid Kr and Xe respectively. The very large value of C in Cu_2O is partly due to the exciton-phonon interaction. To correct for this effect we have to consider Eq. (A2). The dielectric constant ε takes into account screening of the electron-hole Coulomb interaction from both the electrons and the phonons in the crystal. If the exciton radius is large ε is usually taken to be equal to the static dielectric constant ε_o (i.e. all electrons and phonons contribute to ε). When the exciton radius becomes comparable to the lattice constant the phonons can no longer screen effectively the Coulomb interaction between the electron and hole and ε approaches ε_∞ (i.e. only electrons contribute to ε). Various

models have been proposed to calculate this dependence of ε on the exciton radius.[31,37] Here we will be contented to obtain an estimate of the maximum correction to C due to exciton-phonon interaction.

This can be done by noting that $B \propto \varepsilon^{-2}$. The maximum and minimum values B can take (assuming μ to be constant) correspond to $\varepsilon = \varepsilon_\infty$ and $\varepsilon = \varepsilon_o$ respectively. The maximum correction to C due to exciton-phonon interaction is obtained if we assume $\varepsilon = \varepsilon_\infty$ for the 1s yellow exciton and $\varepsilon = \varepsilon_o$ for the $n \geq 2$ levels. In other words the maximum binding energy of the 1s yellow exciton is given by

$$B' = \left(\frac{\varepsilon_o}{\varepsilon_\infty}\right)^2 B \qquad \text{(A5)}$$

Using the experimental values of $\varepsilon_o(7.4)$ and $\varepsilon_\infty(6.5)$ for Cu_2O[13] and Eq. (A5) we find the exciton-phonon interaction correction can at most reduce C to 0.1, still comparable to, say, solid Kr. Thus 0.1 represents the <u>minimum</u> value of C for Cu_2O without central-cell correction.

The purpose of the above discussion is to show the importance of central-cell correction in the 1s yellow exciton. One can arrive at the same conclusion by slightly different arguments. Although the 1s exciton radius has not yet been measured directly, it is possible to estimate its magnitude using the hydrogenic model. By combining Eq. (A2) and (A3) we obtain Eq. (43) in Section IV:

$$a_o = (2\ \varepsilon\ B)^{-1}$$

Instead using the value of B obtained from Eq. (1) we used the experimental value for the 1s exciton and $\varepsilon = \varepsilon_o$ in Eq. (43). In this way we obtained $a_o \sim 7$ Å as compared to the lattice constant of 4.26 Å. With a_o comparable to the lattice constant, one expects central-cell correction

to be important for Cu_2O.

A formalism for studying central-cell corrections to the exciton binding energy has been proposed by Hermanson and Phillips[38] and applied quite successfully to solid Kr and Xe by Hermanson.[39] However, we are not aware of any attempt to apply such corrections to exciton effective mass. In the absence of any applicable theory we have appealed to simple physical agruments in the following qualitative analysis.

The magneto-absorption measurements of Zhilich et al.[30] determined the effective masses, m_e and m_h, of the electron and hole forming the 1s yellow exciton. In our RRS experiment we obtained M^{-1}, the curvature of the 1s exciton band. The hydrogenic model (or effective mass approximation) neglects the periodic crystal lattice and treats the electron and hole as free particles (the crystal field effect is included only in the effective mass). Thus within this model M is equal to m_e+m_h. This approximation is valid when the electron and hole are not strongly localized with respect to each other so that only electrons and holes close to the zone center (where a parabolic expansion is valid) are involved in forming the exciton.[40] When the electron and hole are strongly localized as in the 1s yellow exciton, the entire band structure of the crystal has to be taken into account. In other words the energy of the electron contains terms in k^4, k^6 etc. in addition to $\hbar^2k^2/2m_e$.[38] These higher order terms tend to make the electron appear heavier in forming the exciton. The reason is that, due to the crystal's cellular structure, the bands are flattened at the zone boundaries and the band widths are reduced from that of the parabolic bands. From the point of view of the tight-binding approximation, this reduction in band width is equivalent to an increase in the mass. Hence, we expect that when central-cell corrections are intro-

duced to take into account the real band structure of Cu_2O, the mass of the 1s exciton, M, will be larger than $m_e + m_h$.

Obviously further theoretical work is required to provide a quantitative verification of the above arguments and we hope our work will provide the stimulus for such investigations.

REFERENCES

1. A reveiw article has been written recently by R. M. Martin and L. Falicov (to be published).

2. See for example J. F. Scott, R.C.C. Leite and T. C. Damen, Phys. Rev. 188, 1285 (1969).

3. O. G. Peterson, S.A. Tuccio and B. B. Snavely, Appl. Phys. Letters 17, 245 (1970); M. Hercher and H. A. Pike, Optics Comm. 3, 65 (1971).

4. P. Y Yu, Y. R. Shen, Y. Petroff and L. Falicov, Phys. Rev. Letters, 30, 283 (1973).

5. P. Y. Yu and Y. R. Shen, Phys. Rev. Letters 32, 373 (1974).

6. P. Y. Yu and Y. R. Shen, Phys. Rev. Letters 32, 939 (1974).

7. E. F. Gross, J. Phys. Chem. Solids 8, 172 (1959); Adv. Phys. Sci. (Moscow) 76, 432 (1962).

8. S. Nikitine in Optical Properties of Solids ed. by S. Nudelman and S. S. Mitra (Plenum Press, N.Y. 1969).

9. R. J. Elliot, Phys. Rev. 124, 340 (1961).

10. R. J. Elliot, Phys. Rev. 15, 1384 (1957).

11. P. W. Baumeister, Phys. Rev. 121, 359 (1961).

12. K. Huang, Z. Für Physik 171, 213 (1963); C. Carabatos, Phys. Stat. Solidi 37, 773 (1970); C. Carabatos and B. Prevot, Phys. Stat. Solidi 44, 70 (1971).

13. P. Dawson, M. M. Hargreave and G. R. Wilkinson, J. Phys. Chem. Solids 34, 2201 (1973); J.C.W. Taylor and F. L. Weichman, Canad, J. of Phys.

49, 601 (1971); J. Reydellet, M. Balkanski and D. Trivich, Phys. Stat. Solidi 52b; 175 (1972); M. O'Keefee, J. Chem. Phys. 39, 1789 (1963) and E. C. Heltemes, Phys. Rev. 141, 803 (1966).

14. E. F. Gross and F. I. Kreingol'd, Zh ETF Pis. Red. 7, 281 (1968) [English Translation: JETP Letters 7, 218 (1968)]; A Compaan and H. Z. Cummins, Phys. Rev. B6, 4753 (1972).

15. A. Campaan and H. Z. Cummins, Phys. Rev. Letters 31, 41 (1973); Y. Petroff (unpublished).

16. R. Loudon, Adv. Phys. 13, 423 (1964).

17. W. Heitler, The Quantum Theory of Radiation, 3rd Ed. Oxford University Press (1954).

18. E. Burstein, D. L. Mills, A. Pinczuk and S. Ushioda, Phys. Rev. Letters 22, 348 (1969).

19. C. Carabatos, C. R. Acad, Sci. Ser. B 270, 1289 (1970).

20. A. K. Ganguly and J. L. Birman, Phys. Rev. 162, 806 (1967).

21. D. Trivich and G. P. Pollack, J. Electrochem. Soc. 117, 334 (1970).

22. Y. Petroff, P. Y. Yu and Y. R. Shen (unpublished).

23. R. Loudon, J. Phys. Radium 26, 677 (1965).

24. S. Nikitine, J. B. Grun, M. Certier, J. L. Deiss and M. Grossman, Proc. Int. Conf. on the Phys. of Semiconductors, Exeter 1962, p. 409, The Institute of Physics and Physical Society, London (1962).

25. M. V. Klein, Phys. Rev. B8, 919 (1973).

26. Y. R. Shen, Phys. Rev. B9, 622 (1974).

27. Y. Toyozawa, Prog. Theo. Phys. 20, 53 (1958).

28. J. Hallberg and R. Hanson, Phys. Status Solidi 42, 305 (1970). The LA phonon velocity v used in this paper has been obtained by averaging the LA phonon velocities along the principal symmetry directions.

29. R. M. Martin and C. M. Varma, Phys. Rev. Lett. 26, 1241 (1971).

30. A. G. Zhilich, J. Halpern, and B. P. Zakharchenya, Phys. Rev. 188, 1294 (1969).

31. H. Haken, J. Phys. Chem. Solids 8, 166 (1959).

32. R. C. C. Leite, J. F. Scott and T. C. Damen, Phys. Rev. Letters 22, 780 (1969); M. V. Klein and S.P.S. Porto, Phys. Rev. Letters 22, 782 (1969).

33. S. Nikitine, J. Schmitt-Burckel, J. Biellman and J. Ringeissen, J. Phys. Chem. Sol. 35, 951 (1964).

34. L. Nosenzo, E. Reguzzoni and G. Samoffia, Phys. Rev. Lett. 28, 1388 (1972).

35. G. Baldini, Phys. Rev. 128, 1592 (1962).

36. J. C. Phillips in The Optical Properties of Solids ed. by J. Tauc (Academic Press, N.Y. 1966).

37. S. D. Mahanti and C. M. Varma, Phys. Rev. 6, 2209 (1972). K. K. Bajaj, Solid State Comm. 15, 1221 (1974).

38. J. Hermanson and J. C. Phillips, Phys. Rev. 150, 652 (1966).

39. J. Hermanson , Phys. Rev. 150, 660 (1966).

40. See for example. R. S. Knox, Theory of Excitons (Academic Press, N.Y. 1963).

FIGURE CAPTIONS

1. Absorption spectrum of Cu_2O at 4.2°K showing the yellow excitonic series and the phonon-assisted absorption edge (from Ref. 11).

2. Diagrammatic representations of two-phonon Raman processes. The notations are ----------photon, ~~~~~~~~ phonon, _____ electron-hole pair, o electron-photon interaction, ■ electron-one phonon interaction and □ electron-two phonon interaction.

3. Schematic diagram of the apparatus used in resonance Raman scattering.

4. Raman spectra of Cu_2O for three different incident laser frequencies; (a) 16 470 cm^{-1}, (b) 16 528 cm^{-1} and (c) 16 864 cm^{-1}. The peak E_1 is a luminescence line (see Ref. 22).

5. The Raman cross-section of the $2\Gamma_{12}^-$ (220 cm^{-1}) mode of Cu_2O plotted as a function of incident photon energies. The broken line is a plot of Eq. (27).

6. The Raman cross-section of various two-phonon modes of Cu_2O plotted as a function of incident photon frequencies. + $2\Gamma_{12}^-$ mode, o $\Gamma_{12}^- + \Gamma_{25}^-$ mode, $\Delta\Gamma_{12}^- + \Gamma_{15}^{-(1)}$ mode, • $\Gamma_{12}^- + \Gamma_{12}^-$ mode, □ $\Gamma_{12}^- + \Gamma_{15}^{-(2)}$ (TO) mode and ■ $\Gamma_{12}^- + \Gamma_{15}^{-(2)}$ (LO) mode. The solid curves drawn through the data points are for guidance of eyes only.

7. The Raman cross-section of three- and four-phonon modes of Cu_2O plotted as a function of incident photon frequencies: ..+...+....$2\Gamma_{12}^- + \Gamma_{25}^-$ mode, -.-o.-o.-$3\Gamma_{12}^-$ mode, Δ $2\Gamma_{12}^- + \Gamma_{15}^{-(1)}$ mode and ...•...•....$4\Gamma_{12}^-$ mode. The solid line is a theoretical curve (see text).

8. Raman frequency shifts of all the observed Raman modes of Cu_2O between 190 and 400 cm^{-1} as a function of incident photon energy ω_ℓ. The broken curves are drawn for clarity. The solid curves are theoretical curves discussed in the text. The vertical bars over the experimental points indicate the half-widths of the corresponding Raman peaks. The position of the absorption edge $\omega_1^0 + \omega_{12}$ is indicated by an arrow.

9. Diagrammatic representations of various scattering processes in Cu_2O involving the 1s yellow exciton:
   (a) Phonon-assisted excitation of the 1s yellow exciton:
   (b) RRS of two-phonon mode X+Y with 1s yellow exciton as resonant intermediate state;
   (c) radiative recombination of the 1s yellow exciton;
   (d) intraband scattering of the 1s yellow exciton by one phonon;
   (e) intraband scattering of the 1s yellow exciton by two Γ_{12}^- phonons;
   (f) RRS of the $2\Gamma_{12}^-$ + LA mode;
   (g) RRS of the $2\Gamma_{12}^-$ + P mode with the 1s yellow exciton as intermediate state;
   (h) RRS of the $4\Gamma_{12}^-$ mode.

10. Lineshape of the $2\Gamma_{12}^-$ + LA (referred to as the peak Y in the text) mode of Cu_2O for four incident photon frequencies: (a) 16 560 cm^{-1} (b) 16 724 cm^{-1} (c) 16 772 cm^{-1} and (d) 16 818 cm^{-1}. The dotted curves are plots of Eq. (38) with M as an adjustable parameter. The values of M used in the different curves are: (a) 2.8 m_o (b) 2.9 m_o (c) 3.0 m_o and (d) 2.9 m_o.

11. Peak Raman cross-section of the $2\Gamma_{12}^-$ + LA mode (Y) of Cu_2O as a function

of incident photon frequencies. The solid curve is a theoretical curve discussed in text.

12. Lineshape of the $2\Gamma_{12}^{-}$ + 2LA mode (referred to as the peak Z in the text) of Cu_2O for four incident photon frequencies: (a) 16 632 cm^{-1}, (b) 16 587 cm^{-1} (c) 16 570 cm^{-1} and (d) 16605 cm^{-1}. The broken curves are plots of Eq. (45) with the peak height as the only adjustable parameter.

TABLE I. PHONON ENERGIES OF Cu_2O OBTAINED BY VARIOUS TECHNIQUES

Symmetry Assignment of Phonons	Phonon Energies (cm^{-1}) Obtained by Infrared[a] Absorption (Room Temp.)	Optical[b] Absorption	Raman[c] Scattering	Luminescence[d]	Theoretical[e] Calculation
Γ_{25}^-		88	86	87	98.6
Γ_{12}^-		110	109	110	110
$\Gamma_{15}^{-(1)}$ (TO)	146.3		153	152	143
$\Gamma_{15}^{-(1)}$ (LO)	149.3			154	159
Γ_2^-			350	350	307
Γ_{25}^+			515	515	549
$\Gamma_{15}^{-(2)}$ (TO)	609		640	633	608
$\Gamma_{15}^{-(2)}$ (LO)	638		660	662	639

[a] From Ref. 13.

[b] From S. Brahms and M. Cardona, Solid State Communications 6, 733 (1968).

[c] From Refs. 4,5 and 15.

[d] From Refs. 22.

[e] From Ref. 12.

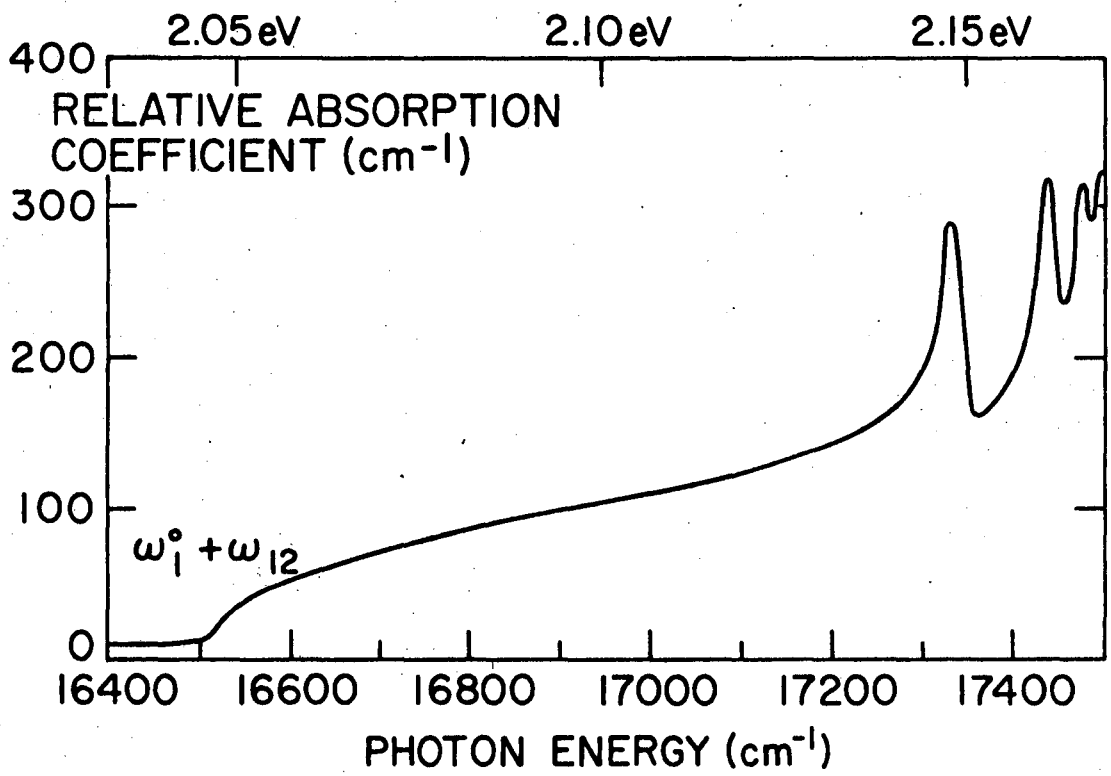

Figure 1

Fig. 1

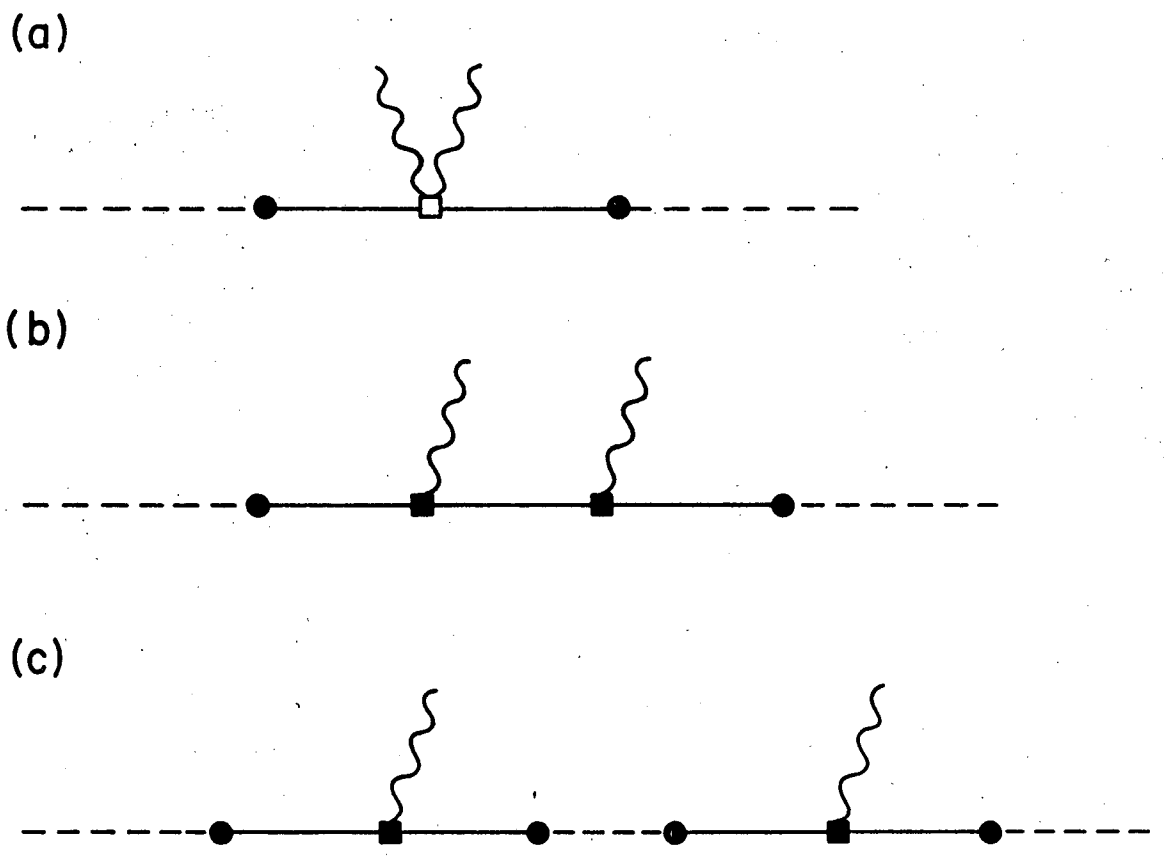

Fig. 2

Figure 2

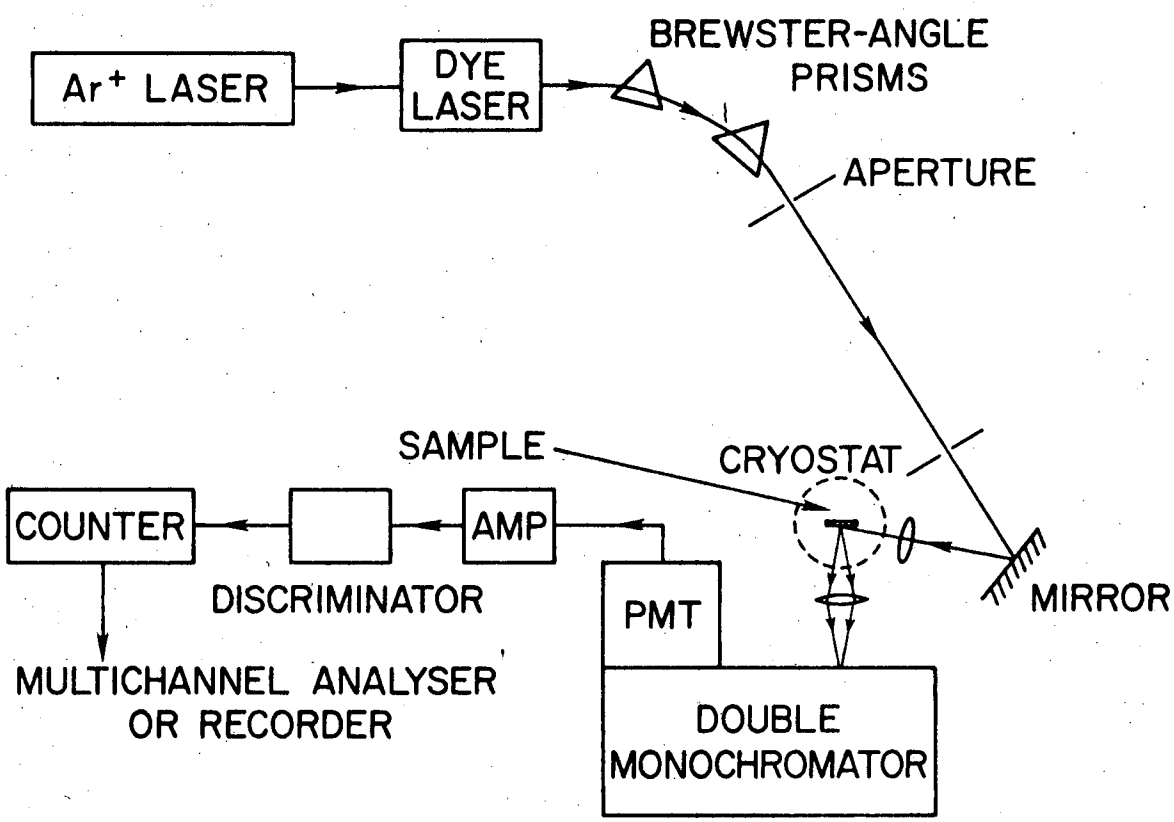

Fig. 3

Figure 3

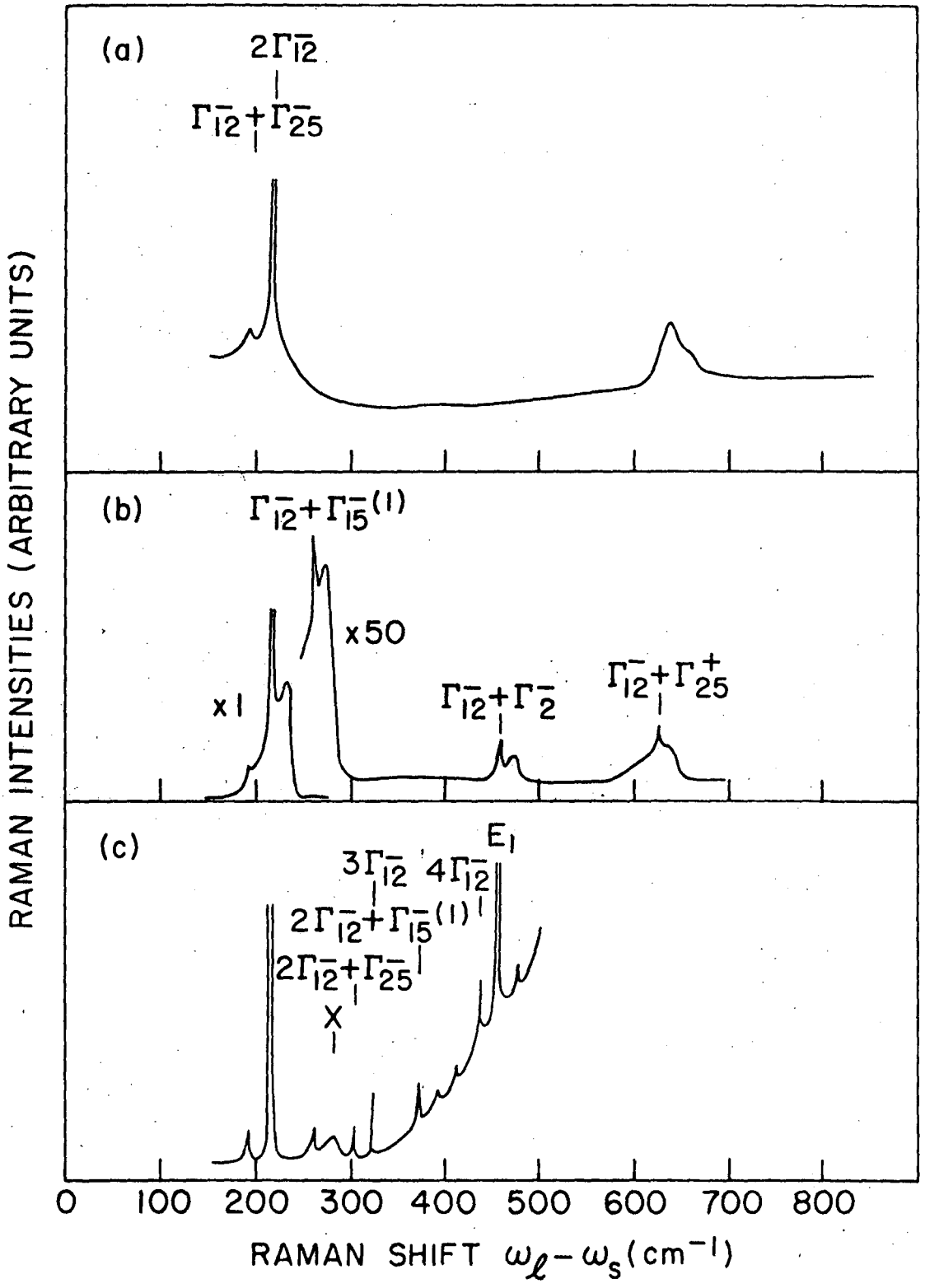

Fig. 4

Figure 4

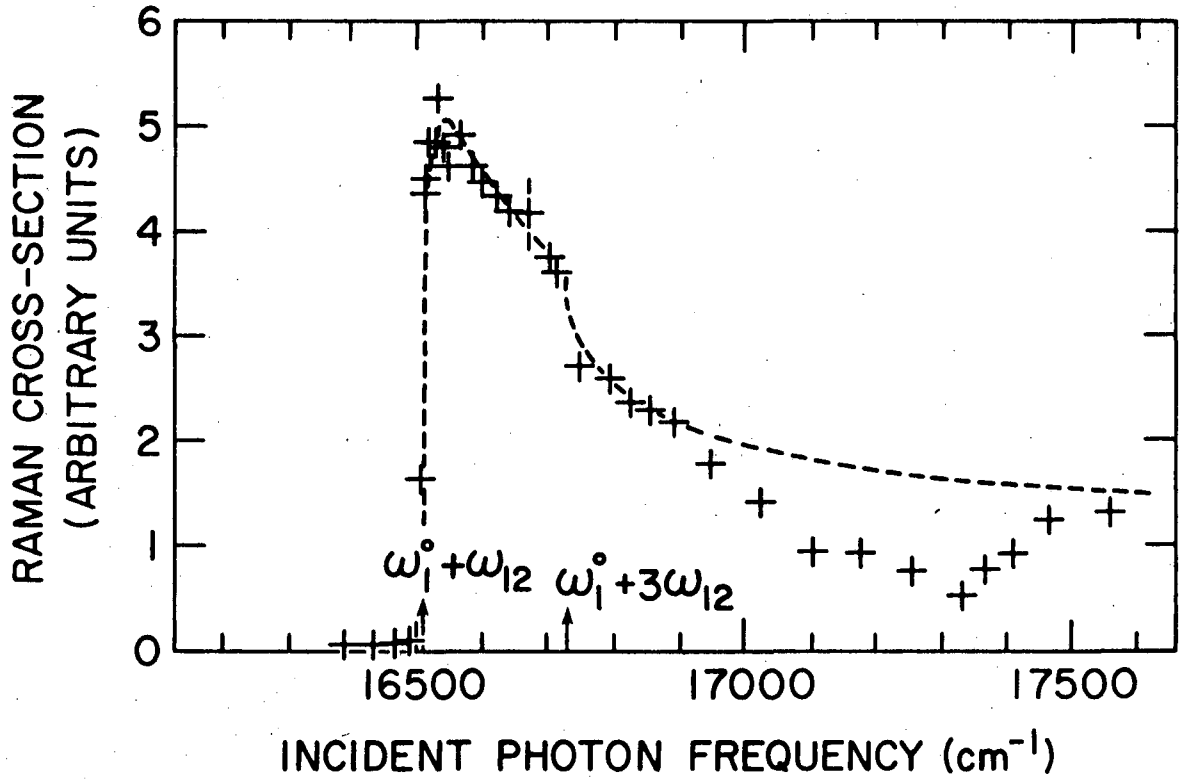

Figure 5

Fig. 5

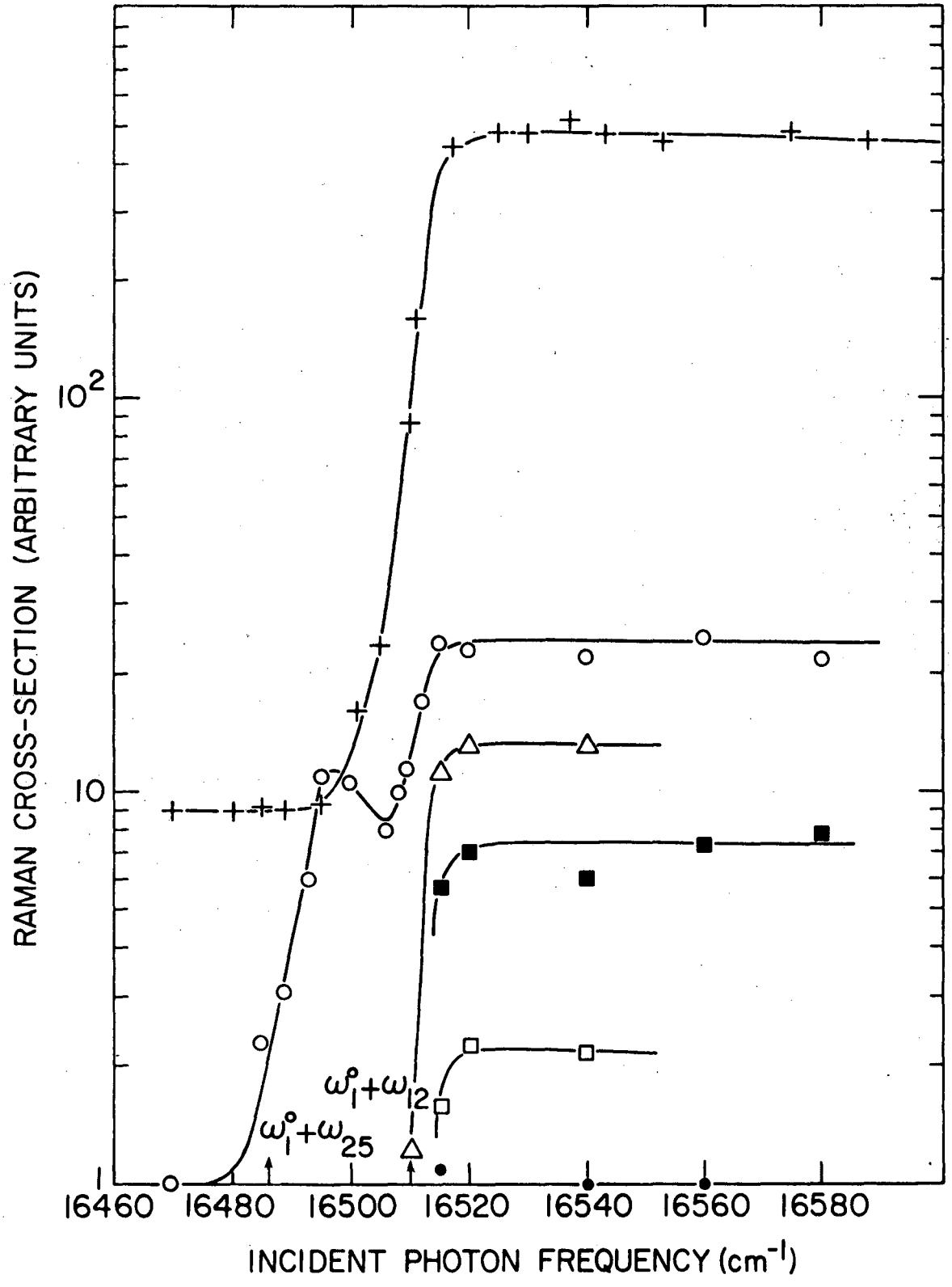

Fig. 6

Figure 6

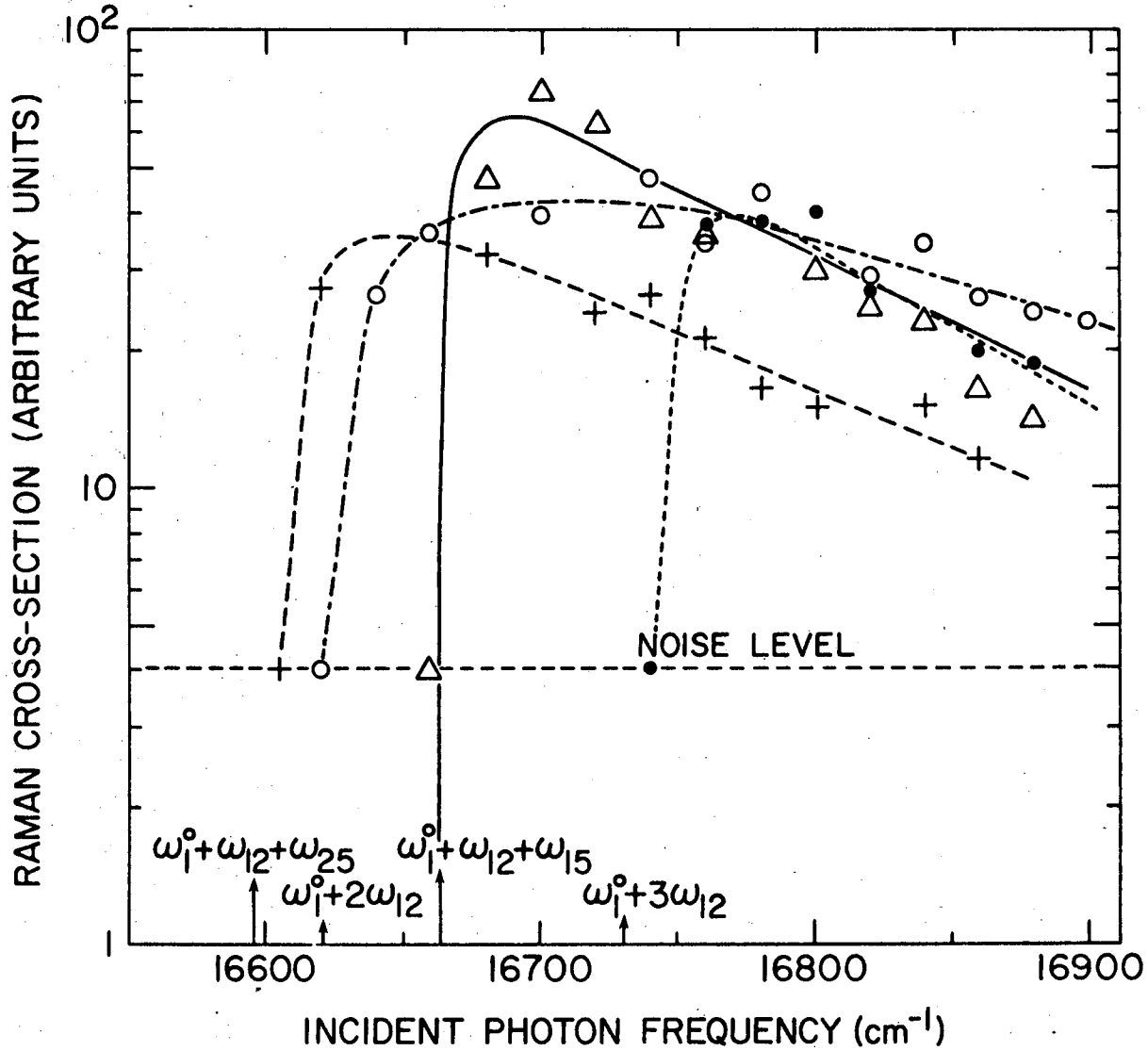

Fig. 7

Figure 7

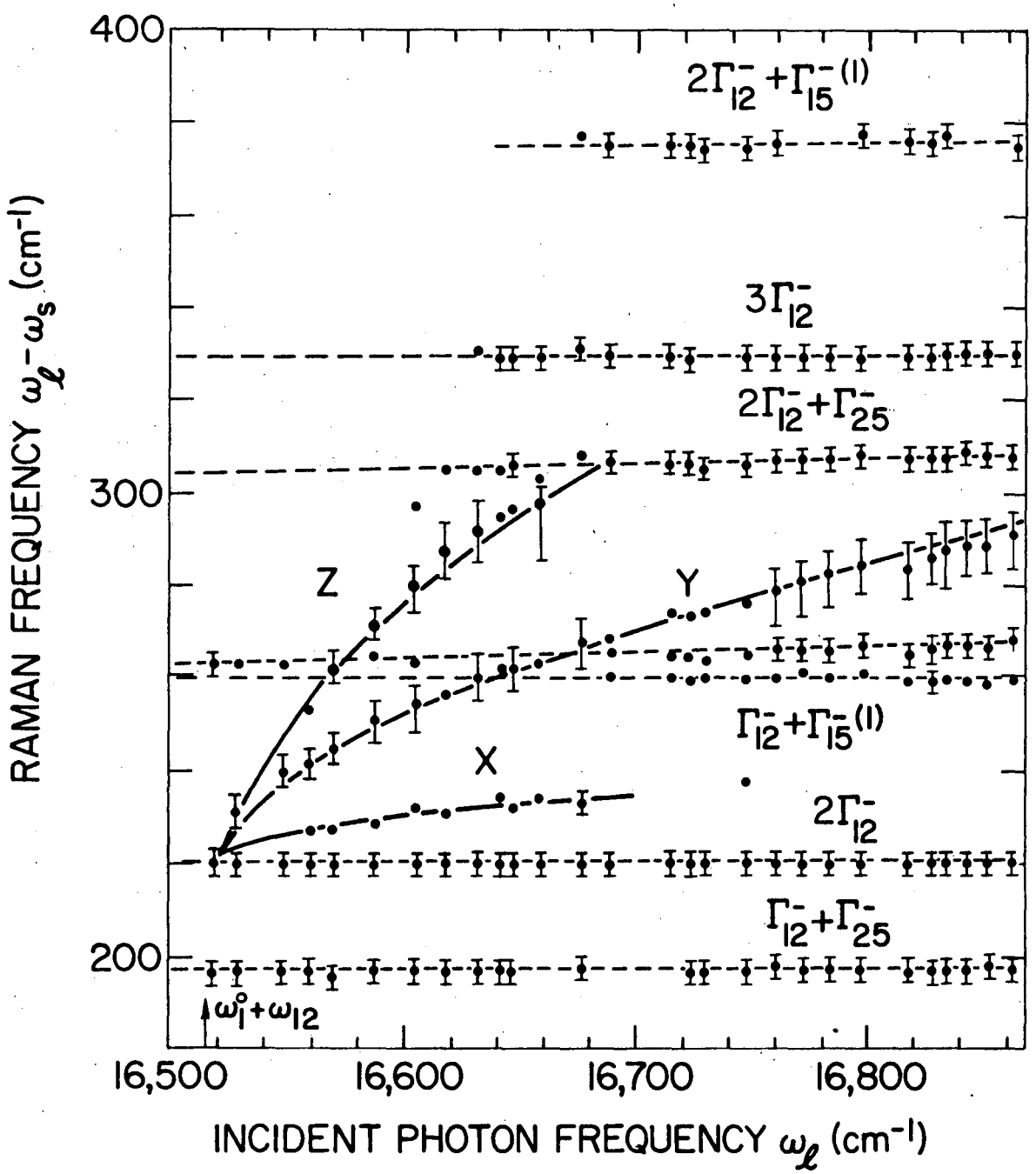

Fig. 8

Figure 8

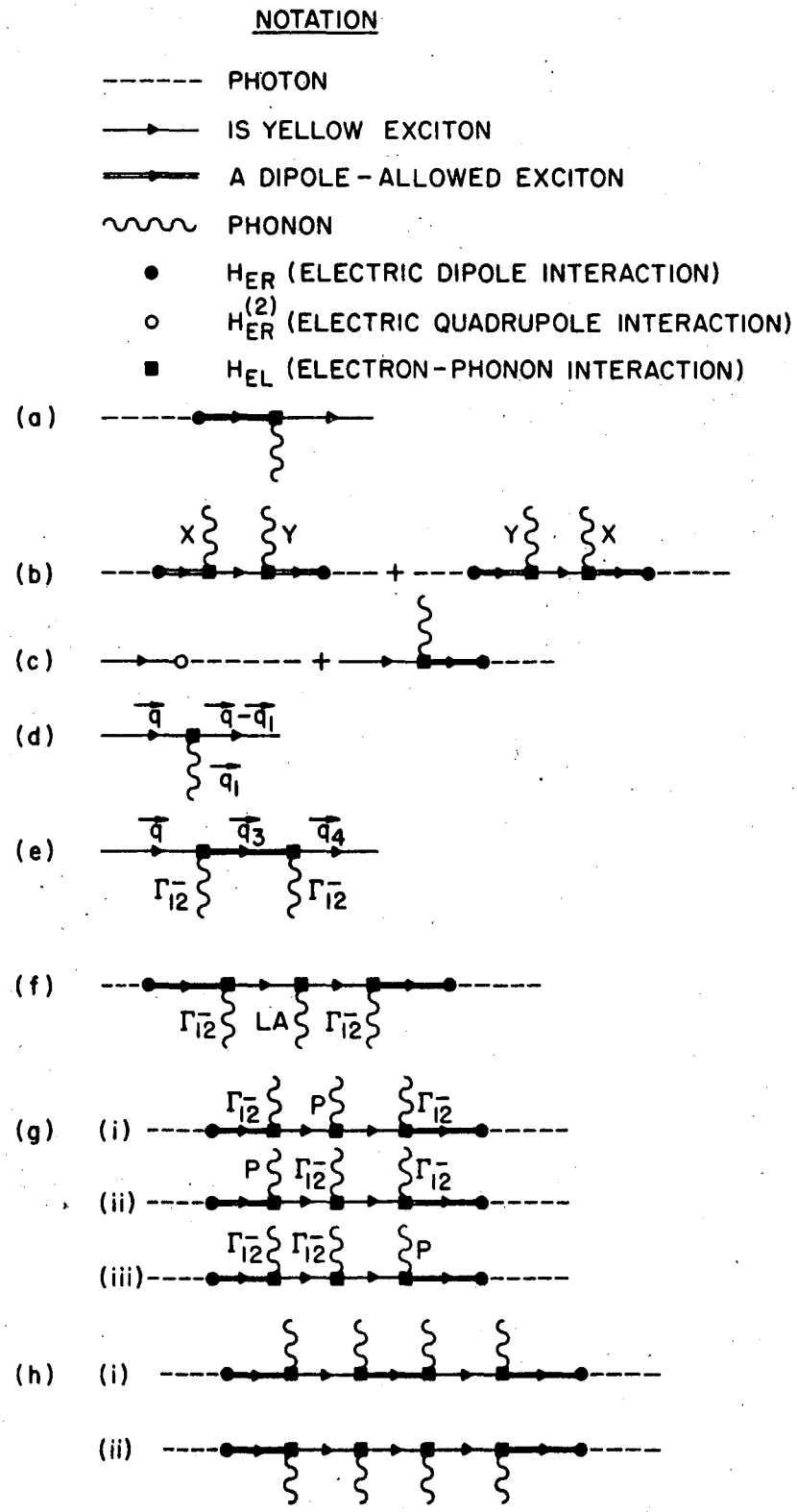

Figure 9

Fig. 9

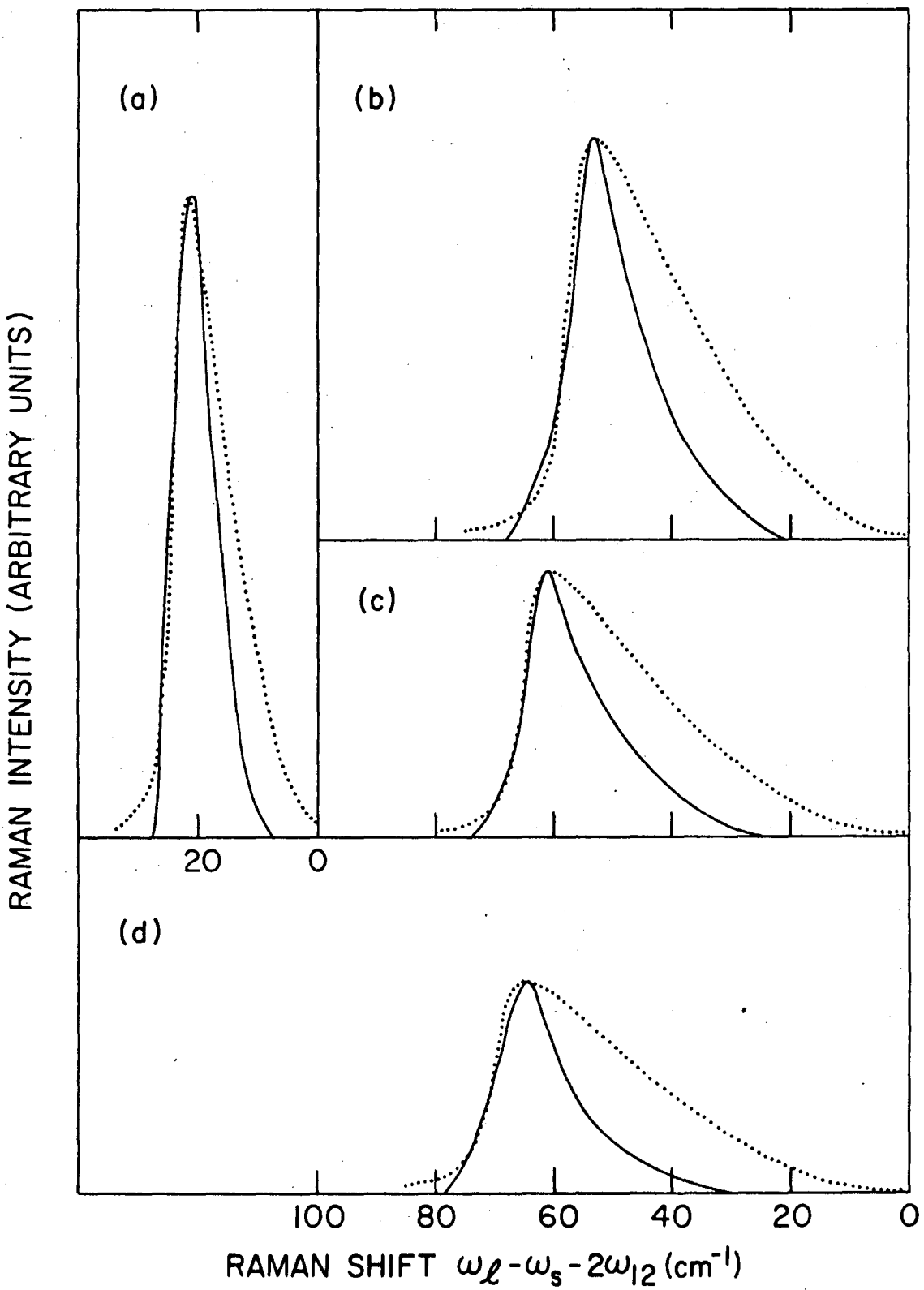

Fig. 10

Figure 10

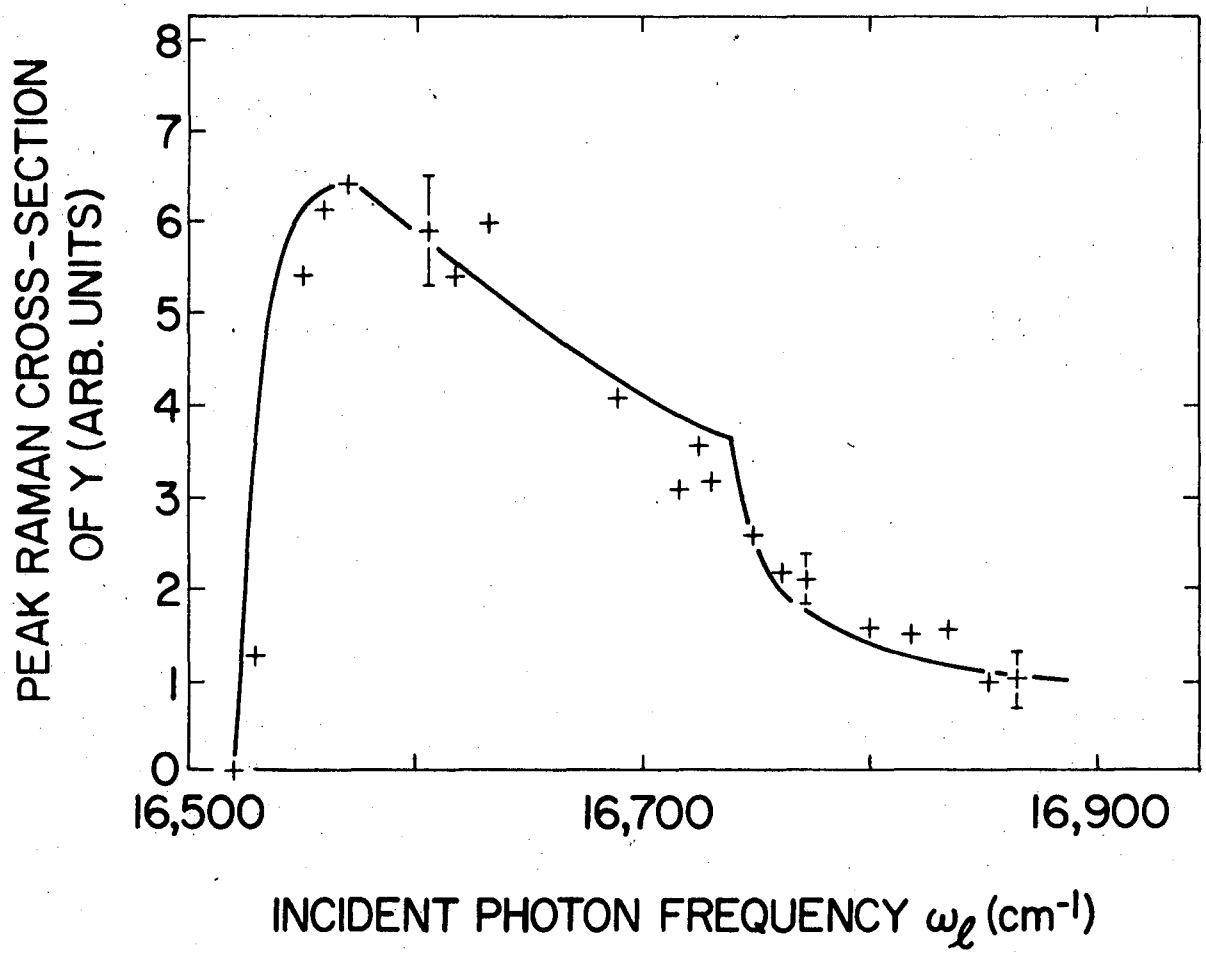

Fig. 11

Figure 11

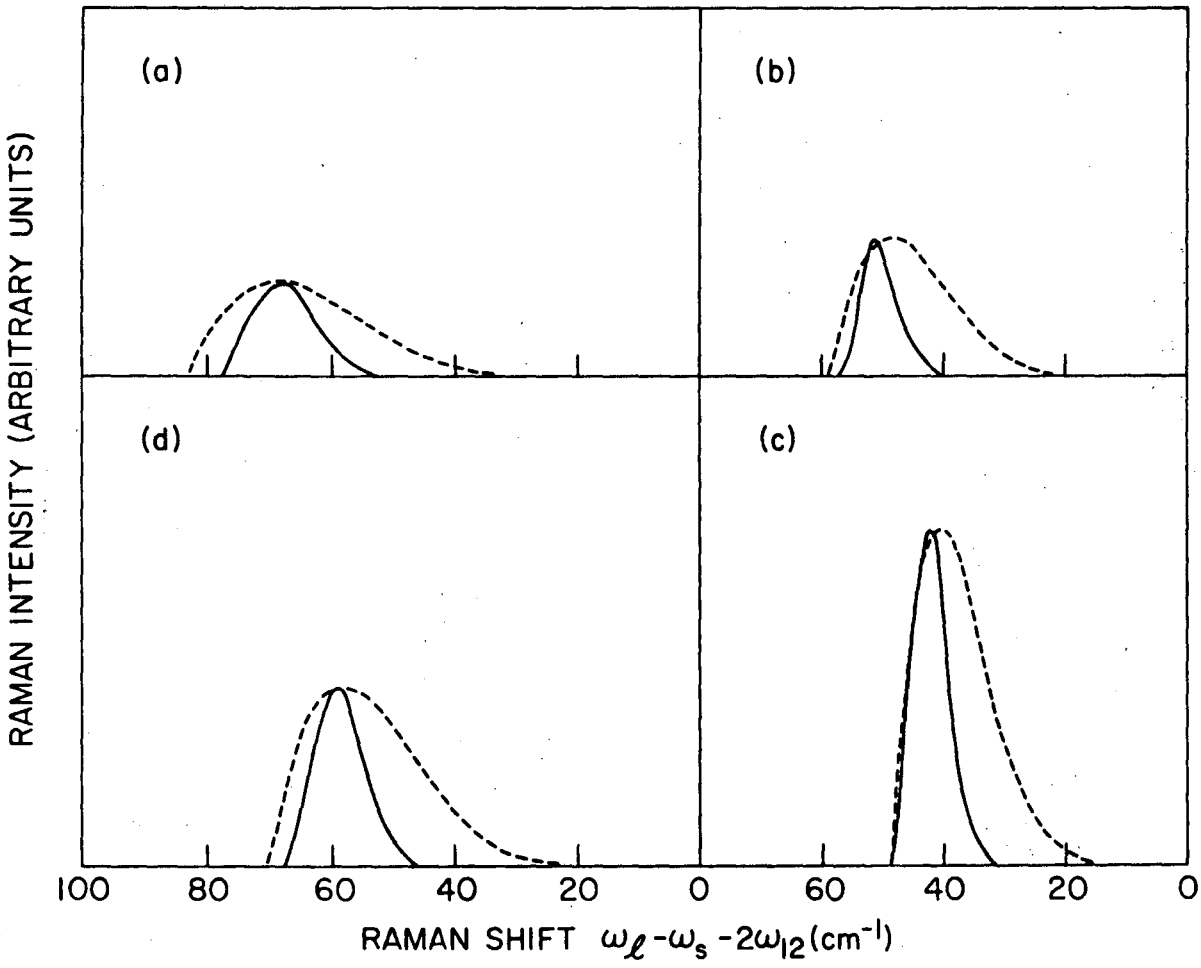

Fig. 12

Figure 12.

TECHNICAL INFORMATION DIVISION
LAWRENCE BERKELEY LABORATORY
UNIVERSITY OF CALIFORNIA
BERKELEY, CALIFORNIA 94720